TET1 non-catalytic activity shapes the chromatin landscape associated with de novo methylation establishment in the male germline

Prasasya, R. D.[1], Kim, J. J.[1], Liu, Z.[1], Kohli, R. M.[2,3], Bartolomei, M. S.[1,3]

[1]Department of Cell and Developmental Biology, Perelman School of Medicine, University of Pennsylvania, Philadelphia, PA 19104, USA

[2]Department of Medicine, Perelman School of Medicine, University of Pennsylvania, Philadelphia, PA 19104, USA

[3]Penn Epigenetics Institute, University of Pennsylvania, Philadelphia, PA, 19104, USA

*Correspondence: bartolom@pennmedicine.upenn.edu (MSB)

Abstract

In the germline, DNA methylation is globally erased in primordial germ cells (PGCs), enabling establishment of sex-specific methylomes in prospermatogonia or oocytes. The catalytic activity of TET1 is required for complete demethylation in PGCs, yet sperm from *Tet1*$^{-/-}$ mice display methylation defects not explained by incomplete erasure. Instead, these defects arise from abnormal *de novo* methylation during development, coinciding with erosion of H3K4me3, a chromatin modification that blocks DNMT3A/3L. Using a catalytically inactive *Tet1*^{HxD} mouse line, we demonstrate a non-catalytic role of TET1 in promoting H3K4me3 deposition and protecting a subset of sperm hypomethylated regions from aberrant methylation in prospermatogonia.

23 **Introduction**

24 DNA methylation is one of the most sexually dimorphic epigenetic marks in mammalian
25 gametes (Stewart et al. 2016). Following specification from cells of the proximal epiblast,
26 primordial germ cells (PGCs) undergo epigenetic reprogramming that involves both chromatin
27 remodeling and genome-wide DNA methylation erasure (Saitou et al. 2005; Smith and Meissner
28 2013; Saitou et al. 2011; Hajkova et al. 2002, 2008). In the mouse developmental timeline, the
29 PGC genome attains a hypomethylated state by embryonic day (E)13.5 (Seisenberger et al.
30 2012). From this common basal epigenetic state, the sperm genome becomes highly
31 methylated (~90% overall methylation in the mouse) while the oocyte genome remains
32 intermediate, with distinct hyper- and hypomethylated domains (Kobayashi et al. 2012; Hanna et
33 al. 2018). In the male germline, acquisition of DNA methylation occurs in prospermatogonia
34 between E15.5 and postnatal day 0. In contrast, *de novo* methylation occurs postnatally in
35 oocytes when individual follicles are recruited for growth during each estrus cycle. Despite the
36 distinct timing and the divergent resulting methylomes between the two sexes, *de novo* DNA
37 methylation is facilitated by a common DNA methyltransferase (DNMT) complex: DNMT3A and
38 its noncatalytic co-factor DNMT3L (DNMT3A/3L) (Kaneda et al. 2004; Kato et al. 2007;
39 Bourc'his and Bestor 2004; Dura et al. 2022).

40 The mechanisms that target DNMT3A/3L to distinct loci in prospermatogonia versus the
41 growing oocyte to generate sex-specific methylomes are still unclear. Biochemical studies
42 suggest crosstalk between histone post-translational modifications (PTMs) and genome
43 accessibility for DNMT3A/3L. For example, the PWWP domain of DNMT3A binds to di- or tri-
44 methylated H3K36 (H3K36me2/me3) (Dhayalan et al. 2010). In the germline, H3K36me2
45 enriched domains are highly correlated with DNA methylation acquisition in prospermatogonia
46 while transcription-coupled H3K36me3 deposition directs DNMT3A/3L and is the rate-
47 determining chromatin environment in oocyte *de novo* methylation (Shirane et al. 2020; Chotalia
48 et al. 2009; Stewart et al. 2015). In contrast, biochemical and *in vitro* studies have shown that

methylation of H3K4 (H3K4me1/2/3) repels the ADD domain of DNMT3A and DNMT3L, inhibiting DNA methylation activity (Zhang et al. 2010; Ooi et al. 2007). In the male germline, DNA methylation acquisition occurs broadly, except at regions enriched for H3K4me2 at the prospermatogonia stage (Singh et al. 2013) . Our previous data also confirmed the high congruency of H3K4me3 enrichment in prospermatogonia with sperm hypomethylated regions (HMRs, regions identified as methylation canyons using high coverage whole genome bisulfite sequencing of the sperm genome) (Prasasya et al. 2024). A functional study targeting writers for H3K4 methylation in the context of male *de novo* methylation has yet to be done, likely owing to the concern for potential functional redundancies of various histone methyltransferases expressed at high levels in prospermatogonia (Zhao et al. 2021). Additionally, how the prospermatogonia or the oocyte genome is patterned for H3K36me2/3 or H3K4me1/2/3 prior to gametic *de novo* methylation establishment remains unresolved.

In our previous investigation of the methylcytosine dioxygenase, Ten-eleven translocation 1 (TET1), in germline reprogramming, we described extensive methylation defects in *Tet1*$^{-/-}$ sperm beyond the previously described limited numbers of TET1-dependent loci (i.e. imprinting control regions -ICRs- and meiosis-associated gene promoters that require TET1 during PGC epigenetic reprogramming) (Prasasya et al. 2024; Yamaguchi et al. 2012, 2013; Hill et al. 2018; SanMiguel et al. 2018). TET enzymes iteratively oxidize 5-methylcytosine (5mC) to 5-hydroxymethylcytosine (5hmC), 5-formylcytosine (5fC), and 5-carboxylcytosine (5caC) (Ito et al. 2011). 5hmC is poorly recognized by maintenance DNMT1, while 5fC and 5caC can be excised by thymine DNA glycosylase (TDG) resulting in an abasic site, activating the base excision repair machinery to recover unmodified cytosine (Kohli and Zhang 2013). Using mouse models harboring 5hmC-stalling (diminished activity in generating 5fC/5caC) TET1^{V} and catalytically inactive TET1^{HxD}, we established the necessity of TET1 iterative oxidative capability in germline epigenetic reprogramming. Intriguingly, only a small portion of methylation defects observed in *Tet1*$^{-/-}$ sperm can be attributed to the loss of TET1 catalytic activity. In fact,

75 expression of full-length, catalytically compromised TET1 ($TET1^{HxD}$) was sufficient to rescue
76 about 2/3 of methylation defects observed in *Tet1*$^{-/-}$ sperm (Prasasya et al. 2024). In addition to
77 the catalytic core located within the C-terminus, TET proteins possess an extensive N-terminus
78 with the ability to interact with and recruit several histone modifiers such as OGT, Sin3a, and
79 PRC2 *in vivo* (Vella et al. 2013; Zhu et al. 2018; Wu et al. 2011; Chrysanthou et al. 2022). Here,
80 we demonstrate that the majority of hypermethylation in *Tet1*$^{-/-}$ sperm arises from abnormal *de*
81 *novo* methylation and coincides with diminished H3K4me3 at intergenic hypomethylated
82 regions. Importantly, catalytically inactive TET1 was sufficient to revert the majority of H3K4me3
83 defects observed in *Tet1*$^{-/-}$ germline to WT levels, establishing a non-catalytic role for TET1 in
84 shaping the chromatin landscape of the male germline.
85
86 **Results and Discussion**
87 We conducted global DNA methylation analysis of *Tet1*$^{-/-}$ and WT (*Tet1*$^{+/+}$) PGCs at the
88 completion of reprogramming, E13.5, using the mouse Illumina Infinium Methylation BeadChip.
89 Consistent with previous reports, the *Tet1*$^{-/-}$ PGC genome was not globally hypermethylated
90 compared to WT (Supplemental Fig. S1A) (Yamaguchi et al. 2013; Hill et al. 2018). Aberrantly
91 methylated regions in *Tet1*$^{-/-}$ PGCs were almost exclusively hypermethylated and enriched for
92 ICRs (Figure 1A, Supplemental Fig. S1B, Supplemental Table S1A; 1049 hypermethylated
93 differentially methylated regions -DMRs-, 1 hypomethylated DMR; each DMR corresponds to a
94 single probe on the array). Gene ontology (GO) analysis revealed that hypermethylated DMRs
95 were enriched for genes involved in meiosis prophase I (Figure 1B), consistent with previous
96 findings by us and others showing that promoter activation requires proper demethylation (Hill et
97 al. 2018; Prasasya et al. 2024). We compared hypermethylated DMRs in *Tet1*$^{-/-}$ PGCs with
98 differentially expressed genes (DEGs) from our previously described RNA-seq (Figure 1C,
99 Supplemental Fig. S1C) (Prasasya et al. 2024). Only DMRs within promoters of meiosis-
100 associated genes corresponded to downregulated expression (Supplemental Fig. S1C),

101 suggesting that the transcriptional consequences of TET1-dependent hypermethylation outside
102 of these meiosis-associated genes may manifest later in germ cell development.
103 To assess whether incomplete DNA methylation erasure during PGC development
104 explains the hypermethylation defects previously reported in *Tet1*$^{-/-}$ sperm (Prasasya et al.
105 2024), we compared hypermethylated DMRs at the two stages (Figure 1D-E, Supplemental
106 Table S1B). 348 DMRs were hypermethylated in both *Tet1*$^{-/-}$ PGCs and sperm. As shown in the
107 distribution plot (Figure 1E, panel iii, Supplemental Table S1E), average methylation levels of
108 these regions were unchanged between sperm and PGCs for both genotypes, suggesting that
109 only a small fraction (6.18%) of *Tet1*$^{-/-}$ sperm hypermethylation results from incomplete erasure
110 in PGCs. In contrast, the majority of hypermethylated DMRs in *Tet1*$^{-/-}$ sperm showed no change
111 in *Tet1*$^{-/-}$PGCs compared to WT (Figure 1E, panel i-ii), indicating replication-coupled passive
112 dilution of DNA methylation was sufficient to reprogram these loci. Instead, these regions
113 abnormally acquired DNA methylation following successful erasure in *Tet1*$^{-/-}$ germ cells (Figure
114 1E, panel i-ii, Supplemental Table S1C-D).

115 When comparing WT PGCs and sperm, we noted a subset of regions where DMRs
116 typically gain methylation during normal male germline development; in *Tet1*$^{-/-}$, this acquisition
117 was exaggerated, resembling a hypermorphic phenotype (Figure 1E, panel i). In contrast, a
118 second subset of regions typically remained unmethylated in WT sperm but ectopically gained
119 methylation in *Tet1*$^{-/-}$ (Figure 1E, panel ii). Out of the 5283 *Tet1*$^{-/-}$ sperm DMRs that originated
120 from abnormal methylation acquisition, the majority belonged to the category of hypermorphic
121 gain (3667 hypermorphic gain, 1602 ectopic gain, 14 sperm DMRs did not pass filter in the PGC
122 data set). Finally, we identified 701 regions that required TET1 for reprogramming in PGCs but
123 ultimately became fully methylated in both *Tet1*$^{-/-}$ and WT sperm (e.g. paternally methylated
124 ICRs such as *H19* or *IG-DMR*) or sperm HMRs that continued to demethylate as the germ cells
125 resumed mitosis in spermatogonial stem cells (SSCs) (Figure 1E, panel iv, Supplemental Table

126 S1F). Design group enrichment analysis showed hypermorphic gain of DNA methylation
127 following TET1 loss occurred most frequently at enhancers (Supplemental Fig. S1D), while
128 ectopic gain or DNA methylation following TET1 loss most frequently occurred within CpG
129 islands (Supplemental Fig. S1E). Regions with incomplete erasure occurred mainly at ICRs
130 (Supplemental Fig. S1F, ImprintDMR) and those exclusively hypermethylated in *Tet1*$^{-/-}$ PGCs
131 are most enriched for CpG islands (Supplemental Fig. S1G). Overall, these findings suggest
132 that TET1 not only supports epigenetic reprogramming in PGCs but also regulates proper DNA
133 methylation acquisition during male germline development.

134 We hypothesized that abnormal gain of methylation observed in the *Tet1*$^{-/-}$ male
135 germline occurs concurrently with *de novo* methylation establishment and reflects changes in
136 the chromatin landscape in prospermatogonia. To test this, we conducted CUT&RUN for
137 H3K4me3, a histone PTM that inhibits DNMT3A/3L activity, in E17.5 prospermatogonia. We
138 chose E17.5 as a mid-point of global wave of *de novo* methylation that occurs between E15.5
139 and birth in the male germline (Kobayashi et al. 2013; Seisenberger et al. 2012; Singh et al.
140 2013). For both WT and *Tet1*$^{-/-}$, over 50% of identified peaks were located within distal
141 intergenic regions (Supplemental Fig. S2A). Most identified peaks showed overlap between
142 *Tet1*$^{-/-}$ and WT prospermatogonia, although *Tet1*$^{-/-}$ prospermatogonia had fewer consensus
143 peaks compared to WT (67205 vs 95643 peaks; consensus peaks were defined as peaks called
144 in at least 2 out of 3 biological replicates; Supplemental Fig. S2A, B, Supplemental Table S2A,
145 B). Averaged signals across genic regions or intergenic peaks revealed distinct H3K4me3
146 changes in *Tet1*$^{-/-}$ prospermatogonia (Figure 2A). While *Tet1*$^{-/-}$ prospermatogonia showed higher
147 overall H3K4me3 near transcriptional start sites (TSSs), H3K4me3 was markedly lower at
148 intergenic peaks (Figure 2A). Differential enrichment (FDR ≤ 0.05, minimum 1.5-fold change vs
149 WT) identified 22904 regions that lost H3K4me3, mostly intergenic regions, in *Tet1*$^{-/-}$
150 prospermatogonia (Supplemental Fig. S2C, Supplemental Table S3A). In contrast, 10971

151 regions that gained H3K4me3 mapped predominantly within genic regions (Supplemental Fig.
152 S2C, Supplemental Table S3B). Notably, in prospermatogonia, intergenic H3K4me3 signal
153 intensities were comparable to those at TSSs (Figure 2A; Supplemental Fig. S2E-F),
154 underscoring their potential regulatory importance (Guenther et al. 2007) .

155 To gain further insights into likely genomic targets of TET1 during *de novo* methylation,
156 and their relationship to H3K4me3 changes, we used the 5hmC landscape in wild-type
157 prospermatogonia as a proxy for TET1 localization. As prior work has established that TET
158 antibodies can be an unreliable means of determining TET binding in the absence of added
159 epitope tags (PMID: 25886910; 37456851), localizing 5hmC has been utilized as an alternative
160 proxy for TET binding. Building on these observations, we propose that, even in contexts where
161 its primary function is non-catalytic, TET occupancy can be reliable ascertained by mapping
162 5hmC (Yan et al. 2022). To that end, we conducted selective chemical labeling of 5hmC
163 followed by affinity enrichment and sequencing (5hmC-Seal) to localize 5hmC in
164 prospermatogonia (Supplemental Fig. S2E-F) (Song et al. 2011). We tested whether regions
165 with decreased or increased H3K4me3 enrichment in *Tet1*$^{-/-}$ prospermatogonia were significantly
166 enriched for 5hmC-called peaks compared to random expectation using a permutation-based
167 overlap test (Supplemental Fig. S2G). While regions that gained H3K4me3 did not show
168 significant overlap, H3K4me3 depleted regions were significantly enriched for 5hmC-peaks in
169 prospermatogonia (Supplemental Fig. S2G). As an orthogonal approach, we analyzed publicly
170 available base-resolution maps of 5hmC (APOBEC-seq) for prospermatogonia and defined
171 5hmC-high regions as 1kb non-overlapping bins where at least 5 CpGs were present with a
172 minimum average of 10% 5hmC across the bins (GSE186357) (Yan et al. 2022) . Similar to the
173 correlation between H3K4me3 changes and 5hmC peaks from hmC-Seal, 5hmC-high bins
174 strongly overlapped with H3K4me3 depleted regions in *Tet1*$^{-/-}$ prospermatogonia (Supplemental
175 Fig. S2H). These results suggest that erosion of H3K4me3 deposition during *de novo*

176 methylation acquisition in *Tet1*$^{-/-}$ prospermatogonia coincides with high likelihood of TET1
177 localization in WT prospermatogonia. In contrast, the lack of overlap between regions that
178 gained H3K4me3 and 5hmC-high bins implies a less direct relationship to TET1.
179 As we previously showed, H3K4me3 enrichment in prospermatogonia strongly
180 overlapped with sperm HMRs (Figure 2B, Supplemental Fig. S2D) (Prasasya et al. 2024). With
181 TET1 loss, we observed significantly less overlap (in absolute number of sperm HMRs) between
182 E17.5 H3K4me3 peaks and sperm HMRs (Figure 2B). This initial analysis suggested that fewer
183 sperm HMRs were protected by H3K4me3 in *Tet1*$^{-/-}$ prospermatogonia. To follow up, we
184 analyzed the relationship between *Tet1*$^{-/-}$ sperm DMRs and changes to H3K4me3 in *Tet1*$^{-/-}$
185 prospermatogonia. With the caveat that the Infinium array provided methylation data for only a
186 representative subset of the genome, we found strong overlap between regions that lost
187 H3K4me3 in *Tet1*$^{-/-}$ prospermatogonia and hypermethylated DMRs in *Tet1*$^{-/-}$ sperm (Figure 2C).
188 As described above, the majority of *Tet1*$^{-/-}$ sperm hypermethylated DMRs originate from
189 abnormal methylation acquisition following successful DNA demethylation in E13.5 PGCs
190 (Figure 1E). As biochemical studies have shown the antagonism between methylated H3K4 and
191 *de novo* DNMTs, we posit that diminished H3K4me3 in *Tet1*$^{-/-}$ prospermatogonia increases
192 DNMT3A/3L access, leading to aberrant methylation at these regions. Assessing H3K4me3
193 signals and *Tet1*$^{-/-}$ sperm hypermethylated DMR subsets showed that those originating from
194 abnormal methylation (hypermorphic and ectopic) corresponded to regions with H3K4me3
195 erosion in prospermatogonia, while those originating from incomplete methylation erasure did
196 not show changes in H3K4me3 signals (Figure 2D). DMRs specific to *Tet1*$^{-/-}$ PGCs also showed
197 no H3K4me3 changes at the prospermatogonia stage, suggesting a decoupling between the
198 role of TET1 in DNA demethylation during reprogramming and its role in patterning the
199 chromatin for *de novo* methylation acquisition (Figure 2D). Incidences of abnormal methylation
200 gain that coincide with H3K4me3 reduction in *Tet1*$^{-/-}$ prospermatogonia can be found in both
201 genic and intergenic regions (Figure 2E). ICRs such as those from *Nespas/Gnas* locus, where

202 hypermethylation originated from incomplete methylation erasure (Supplemental Fig. S1B), had
203 largely unchanged H3K4me3 in *Tet1*$^{-/-}$ prospermatogonia (Figure 2E).
204 H3K4me3 is highly enriched at TSSs of active genes in eukaryotic cells (Barski et al.
205 2007; Schneider et al. 2004). The relationship between H3K4me3 and gene transcription is
206 chromatin context dependent, with the strongest evidence demonstrating the need for H3K4me3
207 for transcriptional elongation but not initiation (Lauberth et al. 2013; Wang et al. 2023). We
208 assessed the relationship between H3K4me3 changes and gene expression in *Tet1*$^{-/-}$
209 prospermatogonia. While total RNA sequencing revealed many differentially expressed
210 transcripts in *Tet1*$^{-/-}$ prospermatogonia (DEGs: 2035 upregulated, 4772 downregulated;
211 Supplemental Fig. S3A; Supplemental Table S4A), we did not observe any directional
212 correlations to changes in H3K4me3 (Figure 3A, Supplemental Table S4B). Perhaps consistent
213 with the known promiscuity or leakiness of gene expression in the male germline, where up to
214 80% of all protein-coding genes can be detected at any given developmental stage, DEGs are
215 associated with biological processes at much later stages of spermatogenesis (e.g.
216 downregulation of motility-associated genes and upregulation of chromosome segregation
217 during meiosis-associated genes; Supplemental Fig. S3B, C) (Xia et al. 2020). Overall, our data
218 showed that H3K4me3 in prospermatogonia does not direct global gene expression.
219 To explore the regulatory potential of these altered regions across spermatogenesis, we
220 performed chromatin state discovery using ChromHMM. We built segmentation models from
221 publicly available histone PTMs, Pol2, and CTCF ChIP-seq datasets (Supplemental Fig. S3D,
222 Supplemental Table 5) spanning five stages of spermatogenesis: SSCs, differentiated
223 spermatogonia (SPG), pachytene spermatocyte (PS), round spermatid (RS), and sperm. We
224 assigned chromatin states based on Roadmap Epigenomics Consortium conventions
225 (Supplemental Fig. S3D) (Ernst and Kellis 2012) . Regions that gained H3K4me3 in *Tet1*$^{-/-}$
226 prospermatogonia matched canonical TSS, while regions with depleted H3K4me3
227 corresponded to enhancer-like states (Figure 3B). Regions with reduced H3K4me3 in *Tet1*$^{-/-}$

228 prospermatogonia were enriched for long terminal repeats (LTRs) and LINE elements
229 (Supplemental Fig. S3E). Motif enrichment analysis after repeat masking identified recognition
230 sites for methylation sensitive ETS and HOX families of transcription factors (Figure 3C)
231 (Stephens and Poon 2016; Huang et al. 2012). Consistent with potentially serving as promoters
232 that are relevant for male germ line development (Supplemental Fig. S3F), regions that gained
233 H3K4me3 in *Tet1*$^{-/-}$ prospermatogonia contain motifs for DMRT6 binding, a germ cell-specific,
234 methylation sensitive transcription factor that coordinates the mitosis to meiosis transition
235 (Figure 3D) (Zhang et al. 2014).
236 Our findings support the hypothesis that non-catalytic domains of TET1 contribute to
237 H3K4me3 deposition, which may protect intergenic sperm HMRs from *de novo* methylation
238 acquisition. Indeed, emerging evidence shows that non-catalytic domains of TET1 within the C-
239 terminus interact with chromatin modifiers in development and disease (Lian et al. 2016; Joshi
240 et al. 2022). We previously generated a mouse line with the *Tet1*$^{H1654Y,D1656A(HXD)}$ mutation, which
241 produces a catalytically inactive but full-length TET1 protein (Ko et al. 2011; Chrysanthou et al.
242 2022; Caldwell et al. 2021; Prasasya et al. 2024). To test whether non-catalytic TET1
243 expression is sufficient to establish the chromatin landscape associated with proper male
244 germline *de novo* methylation, we analyzed *Tet1*$^{HxD/HxD}$ prospermatogonia.
245 We conducted CUT&RUN for H3K4me3 in *Tet1*$^{HxD/HxD}$ prospermatogonia at E17.5. In
246 support of our hypothesis, the majority of H3K4me3 changes seen in *Tet1*$^{-/-}$ prospermatogonia
247 were absent in *Tet1*$^{HxD/HxD}$ compared to WT (Figure 4A, Supplemental Fig. S4A, Supplemental
248 Table S2C). Of the regions that lost H3K4me3 in *Tet1*$^{-/-}$ prospermatogonia, over 89% (20494 of
249 22904) were reverted to WT levels in *Tet1*$^{HxD/HxD}$ (Figure 4A, Supplemental Fig. S4A,
250 Supplemental Table S3C, D). The genomic distribution of H3K4me3 consensus peaks in
251 *Tet1*$^{HxD/HxD}$ prospermatogonia was comparable to *Tet1*$^{-/-}$ and WT and consistently overlapped
252 with sperm HMRs (Supplemental Fig. S4B-C). At both TSS-centered and intergenic peaks,

253 H3K4me3 signals in *Tet1*$^{HxD/HxD}$ prospermatogonia showed intermediate levels between WT and
254 in *Tet1*$^{-/-}$ (i.e. increased around TSSs and decreased at intergenic peaks; Supplemental Fig.
255 S4D-E).

256 The limited number of regions where H3K4me3 was depleted in *Tet1*$^{HxD/HxD}$
257 prospermatogonia (compared to WT) remained associated with eventual hypermethylated
258 DMRs in *Tet1*$^{HxD/HxD}$ sperm, although the overlap was significantly reduced compared to *Tet1*$^{-/-}$
259 germ cells (Figure 4B-C). Among 5631 hypermethylated DMRs identified in *Tet1*$^{-/-}$ sperm, 3710
260 (~2/3) were not significantly hypermethylated in *Tet1*$^{HxD/HxD}$ sperm (defined as rescued
261 DMRs)(Prasasya et al. 2024). These methylation defects cannot be fully attributed to loss of
262 TET1 catalytic activity. Of note, regions that remained hypermethylated in *Tet1*$^{HxD/HxD}$ sperm are
263 those that require TET1-iterative oxidation capability such as ICRs and promoter of germline
264 responsive genes (Prasasya et al. 2024).

265 We examined how H3K4me3 enrichment in prospermatogonia relates to the rescue of
266 sperm hypermethylation defects in *Tet1*$^{HxD/HxD}$ compared to *Tet1*$^{-/-}$ sperm. First, we assessed the
267 baseline levels of H3K4me3 in WT prospermatogonia for rescued and not-rescued DMRs and
268 found rescued DMRs display modestly higher baseline levels (Figure 4D). Following the loss of
269 TET1, rescued DMRs underwent a greater depletion of H3K4me3 compared to not-rescued
270 DMRs (Figure 4E), resulting in the convergence of H3K4me3 levels between the two subsets in
271 *Tet1*$^{-/-}$ prospermatogonia (Figure 4F). To quantify the extent of H3K4me3 restoration toward WT
272 levels, we calculated the fold-change of H3K4me3 signal in *Tet1*$^{HxD/HxD}$ relative to *Tet1*$^{-/-}$
273 prospermatogonia. The degree of restoration was significantly greater across rescued DMRs
274 than across those that remained hypermethylated (not-rescued; Figure 4G). Ridgeline plots in
275 Figure 4H demonstrate the difference in dynamic range of H3K4me3 regulation in WT, *Tet1*$^{-/-}$,
276 and *Tet1*$^{HxD/HxD}$ between the two DMR subsets. Overall, rescued DMRs exhibit greater
277 susceptibility to H3K4me3 depletion following TET1 loss, but also greater responsiveness in
278 H3K4me3 restoration in the presence of non-catalytic TET1^{HxD}.

279 To test this relationship more formally, we performed permutation-based enrichment
280 analysis to assess whether rescued DMRs preferentially overlapped regions showing reverted
281 H3K4me3 to WT levels in *Tet1*$^{HxD/HxD}$ prospermatogonia (Gel et al. 2015). Both rescued and not-
282 rescued DMRs showed significant enrichment within H3K4me3-reverted peaks in *Tet1*$^{HxD/HxD}$
283 prospermatogonia (Supplemental Fig. S4F-G), but the effect size (Z-score) was markedly higher
284 for rescued DMRs (Figure 4I). Together, these results indicate that non-catalytic full length
285 TET1^{HxD} is sufficient to enhance H3K4me3 deposition overall in prospermatogonia compared to
286 the absence of TET1. Taken together, our findings suggest that the susceptibility of a region to
287 aberrant DNMT3A/3L reflects the extent, and likely timing, of H3K4me3 erosion in *Tet1*$^{-/-}$
288 prospermatogonia during the *de novo* methylation window (illustrated in Figure 4J).
289 In the male germline, hypermethylation is required, in part, to silence retroelements that
290 are toxic for meiosis (Bourc'his and Bestor 2004; Barau et al. 2016). Despite this, certain
291 regions of the mammalian sperm genome resist DNA methylation, including CpG-dense
292 promoters and younger, species-specific transposon subfamilies overlapping regulatory
293 elements (Shirane and Lorincz 2023; Molaro et al. 2011; Erkek et al. 2013). Additionally, low
294 methylation at CpG-dense regions correlates with nucleosome retention during histone-to-
295 protamine exchange, a critical step male gamete maturation (Erkek et al. 2013) . Retained
296 nucleosomes in sperm play a crucial role in patterning chromatin of the early embryo,
297 underscoring the importance of the sperm epigenome beyond spermatogenesis (Fanourgakis et
298 al. 2025). Thus, the integrity of sperm HMRs is essential for both spermatogenesis and
299 potentially embryo viability.
300 We previously demonstrated that most methylation defects from compromised TET1
301 activity occur within sperm HMRs (Prasasya et al. 2024). Iterative oxidation is required at ICRs
302 and meiosis-associated promoters, but these account for only a small fraction of *Tet1*$^{-/-}$ sperm
303 defects. In addition to its role in active demethylation, TET1 has been proposed to protect
304 against DNA re-methylation during epigenetic reprogramming (Hill et al. 2018). However,

305 DNMT3A/3L activity is limited at E14.5, making this role less likely in PGCs. Our findings instead
306 suggest a role for TET1 in preventing abnormal methylation acquisition in prospermatogonia.
307 Aberrant DNA methylation in *Tet1*$^{-/-}$ sperm correlates with erosion of H3K4me3 at the
308 prospermatogonia stage, a chromatin feature that negatively correlates with hypermethylated
309 regions in the male germline and a mark that has been biochemically demonstrated to be the
310 most antagonistic to DNA methyltransferase access (Figure 4J). Consistently, the non-catalytic
311 function of TET1, as tested in *Tet1*$^{HxD/HxD}$ germline, is sufficient to enhance H3K4me3 deposition
312 and partially rescue DNA methylation (Prasasya et al. 2024). Analysis of H3K4me3 enrichment
313 in *Tet1*$^{HxD/HxD}$ prospermatogonia suggests that there are differential dependencies – likely related
314 to both the magnitude and timing of H3K4me3 changes – that influence TET1 non-catalytic
315 functions and antagonism of DNMT3A/3L during *de novo* methylation, as not all regions with
316 H3K4me3 restoration corresponds to rescue of DNA hypermethylation (Figure 4J). It is notable
317 that our model only allows for correlative interpretations for the importance of H3K4me3 in
318 shaping the sperm HMRs landscape. Additional studies to conditionally target H3K4
319 methyltransferases during *de novo* methylation period are needed to determine the governing
320 rule by which DNMT3A/3L is excluded from sperm HMRs.
321 TET proteins interact with chromatin modifiers in many contexts. In embryonic stem cells
322 (ESCs), the non-catalytic function of TET1 shapes bivalency (H3K4me3, H3K27me3) at
323 regulators of mesoderm and trophectoderm lineages by recruiting Polycomb repressive complex
324 2 (PRC2) and Sin3a (Chrysanthou et al. 2022) . TET1 is also a stable binding partner of *O*-
325 GlcNAc transferase (OGT) and is required for OGT-Sin3a-Hcf1 binding to chromatin (Vella et al.
326 2013; Williams et al. 2011). Hcf1 is a key component of the SET1/COMPASS histone
327 methyltransferase complex, a writer for H3K4me2/3. In hematopoiesis, the TET2/3-OGT
328 complex promotes Hcf1 O-GlcNAcylation, leading to SET1/COMPASS assembly, H3K4me3
329 deposition, and gene activation (Capotosti et al. 2011; Deplus et al. 2013). A similar mechanism
330 is plausible in prospermatogonia, as single cell RNA-seq confirms *Ogt* and *Hcfc1* expression in

331 fetal and neonatal germ cells, coinciding with *de novo* methylation (Zhao et al. 2021). TET1
332 recruitment to regions with TET1-dependent H3K4me3 deposition in prospermatogonia is
333 further supported by the strong overlap between 5hmC localization and H3K4me3 depleted
334 regions in *Tet1*$^{-/-}$ prospermatogonia as shown by the finding of 5hmC-Seal analysis
335 (Supplemental Fig. S2G).
336 It is also possible that in addition to promoting H3K4me3 deposition, TET1 may also
337 partially restrain DNA methylation by physically protecting its targets from DNMT3A/3L in
338 prospermatogonia. This is not likely to be the main mechanism of sperm HMRs protection
339 however, as TET1 and DNMT3A antagonism was previously found to be highly context
340 dependent within proximal promoters (Gu et al. 2018). Furthermore, in human ESCs, TET1 and
341 DNMT3A have been shown to co-bind, especially within DNMT3A preference binding regions
342 (Chao et al. 2022). Notably, TET1-dependent sperm HMRs are intergenic and acquire
343 enhancer-like chromatin states throughout spermatogenesis (Figure 2A, 3B). Top enriched
344 motifs in these regions correspond to ETS transcription factors. Significantly, the ETS family of
345 transcription factors are known to interact with and recruit histone acetyltransferases such as
346 CBP and p300, in further support of the potential of intergenic sperm HMRs as regulatory
347 elements (Yang et al. 1998; Goodman and Smolik 2000). We propose that protecting intergenic
348 sperm HMRs from methylation helps establish the enhancer landscape that regulates stage-
349 specific gene expression, particularly during the mitosis-to-meiosis transition (Maezawa et al.
350 2020). Indeed, *Tet1*$^{-/-}$ male mice reproductive defects are attributed to premature aging due to
351 reduced SSCs and progressively worse meiotic defects (Huang et al. 2020). While the
352 mechanism orchestrating chromatin patterning before *de novo* methylation remains unclear, our
353 findings reveal the non-catalytic function of TET1 as a molecular component for establishing
354 sperm HMRs.
355
356

Methods

Mouse models and germ cell collection

All experiments were approved by the Institutional Animal Care and Use Committee of the University of Pennsylvania (protocol number: 804211). Mice were housed in polysulfone cages within a pathogen-free facility under a 12 h light/dark cycle, with ad libitum access to water and standard chow (Laboratory Autoclavable Rodent Diet 5010, LabDiet, St. Louis, MO, USA). *Tet1* knockout mice (Dawlaty et al. 2013) (017358; B6;129S4-Tet1$^{tm1.1Jae}$/J) and *Oct4-GFP* mice (Lengner et al. 2007) (008214; B6;129S4-Pou5f1^{tm2Jae}/J) were obtained from The Jackson Laboratory and backcrossed for at least 10 generations to a C57BL/6J background (000664; B6; The Jackson Laboratory). Catalytically inactive *Tet1^{HxD}* mouse line was generated as described in (Prasasya et al. 2024). The *Oct4-GFP* allele was maintained as homozygous in *Tet1* heterozygote breeders (*Tet1$^{+/-}$*; *Oct4$^{GFP/GFP}$* or *Tet1$^{HxD/+}$; Oct4$^{GFP/GFP}$)*. Primers to determine sex, *Tet1$^{tm1.1Jae}$*, *Tet1^{HxD}*, and *Oct4-GFP* alleles are listed in Supplemental Table S6.

Gonadal tissues from E13.5 and E17.5 embryos (post copulatory plug detection) were dissected and digested into a single-cell suspension using 0.25% trypsin/EDTA for 10 minutes at 37 °C. *GFP^{+}* germ cells were isolated by flow cytometry. For bisulfite mutagenesis and RNA isolation, germ cells were sorted into empty tubes and immediately snap-frozen for storage at -80 °C until processing. For CUT&RUN, sorted cells were collected into chilled PGC medium (DMEM supplemented with 15% FBS, 100 U/mL leukemia inhibitory factor, 5 μM forskolin, 1 ng/mL stem cell factor). Following sorting, dimethyl sulfoxide (DMSO) was added to a final concentration of 10%, and the cells were slow frozen using Mr. Frosty until library preparation.

Genome-wide DNA methylation profiling using Infinium Mouse Methylation BeadChip

Snap frozen germ cell pellet was directly lysed and bisulfite mutagenized using EZ DNA Methylation Direct Kit (Zymo Research) per manufacturer's instructions. Bisulfite mutagenized (BSM) DNA was subjected to low-input whole-genome amplification workflow prior to hybridization to Illumina BeadChip array as detailed in (Lee et al. 2024) (Workflow J). Briefly, BSM DNA underwent 2 rounds of Klenow amplifications (NEB) using random hexamer primers (NEB). For additional details on library preparation and data analysis, see the Supplemental Material. Amplified DNA was cleaned using solid-phase reversible immobilization (SPRI) beads (2x; Beckman Coulter) and concentration was measured with Qubit (Invitrogen).10 μL of BSM DNA library was submitted for hybridization onto the Infinium Mouse Methylation-12v1-0 BeadChip (Illumina) at Children's Hospital of Philadelphia Center for Applied Genomics.

CUT&RUN library preparation

CUT&RUN experiments were performed on samples of 4,000 nuclei isolated per epitope from cryopreserved germ cells as described above using CUTANA ChIC/CUT&RUN kit (EpiCypher). Three biological replicates per genotype were prepared for H3K4me3 (1:100, Cell Signaling Technology antibody 2729) and IgG (1:50, CUTANA Rabbit IgG negative control antibody). Cells were rapidly thawed and counted, followed by nuclei extraction using NE buffer (20 mM HEPES-KOH pH 7.9, 10mM KCl, 0.5 mM fresh spermidine, 0.1% Triton X-100, 20% glycerol plus protease inhibitors). Nuclei were bound to concanavalin A-coated magnetic beads and

397 CUT&RUN was conducted per CUTANA product manual with modifications. CUT&RUN libraries
398 were prepared with NEBNext Ultra II DNA Library Prep Kit for Illumina (NEB). For additional
399 details on library preparation and data analysis, see the Supplemental Material.

400 *Total RNAseq library preparation*

401 Total RNA was extracted from 5000 snap frozen E17.5 germ cells isolated from a single embryo
402 using TRIzol reagent (Invitrogen). RNA integrity number and concentration were assessed using
403 the High Sensitivity RNA ScreenTape for TapeStation system (Agilent Technologies). Ribosomal
404 RNA-depleted total RNA libraries were generated using the SMART-Seq Total RNA Pico Input
405 Kit with UMIs with ZapR Mammalian (Takara Bio) from 5 ng input according to the
406 manufacturer's protocol. Libraries were indexed with NEBNext Multiplex Oligos for Illumina
407 Unique Dual Index Primer Pairs (NEB) and were amplified using SeqAmp DNA Polymerase
408 (Takara Bio). For additional details on library preparation and data analysis, see the
409 Supplemental Material.

410 *5hmC-Seal library preparation*

411 Genomic DNA was isolated from 30,000 snap frozen E17.5 germ cells pooled from multiple
412 embryos using Phenol:Chloroform:Isoamyl Alcohol (25:24:1; Sigma-Aldrich) and ethanol
413 precipitated, followed by resuspension in 10 mM Tris-HCl pH 8.0. 50 ng of genomic DNA was
414 sheared using NEBNext UltraShear (NEB) and was used as input for enrichment of 5-
415 hydroxymethylcytosine using 5hmC-Seal following manufacturer protocol (5hmC Profiling Kit;
416 Active Motif). Sequencing libraries were prepared from both input and enriched fractions using
417 NEBNext UltraII DNA Library Prep Kit for Illumina (NEB).

418 *Data availability*

419 The accession number for raw and processed Illumina Mouse Infinium BeadChip, CUT&RUN,
420 RNA-seq, and 5hmC-Seal data generated in this paper is submitted to GEO with the accession
421 number GSE318256. Any additional information required to reanalyze the data reported in this
422 paper is available from corresponding author upon request.

423

424 References

425 Barau J, Teissandier A, Zamudio N, Roy S, Nalesso V, Hérault Y, Guillou F, Bourc'his D. 2016.
426 The DNA methyltransferase DNMT3C protects male germ cells from transposon activity.
427 *Science* **354**: 909–912.

428 Barski A, Cuddapah S, Cui K, Roh T-Y, Schones DE, Wang Z, Wei G, Chepelev I, Zhao K.
429 2007. High-Resolution Profiling of Histone Methylations in the Human Genome. *Cell* **129**:
430 823–837.

431 Bourc'his D, Bestor TH. 2004. Meiotic catastrophe and retrotransposon reactivation in male
432 germ cells lacking Dnmt3L. *Nature* **431**: 96–99.

433 Caldwell BA, Liu MY, Prasasya RD, Wang T, DeNizio JE, Leu NA, Amoh NYA, Krapp C, Lan
434 Y, Shields EJ, et al. 2021. Functionally distinct roles for TET-oxidized 5-methylcytosine
435 bases in somatic reprogramming to pluripotency. *Mol Cell* **81**: 859-869.e8.

436 Capotosti F, Guernier S, Lammers F, Waridel P, Cai Y, Jin J, Conaway JW, Conaway RC, Herr
437 W. 2011. O-GlcNAc Transferase Catalyzes Site-Specific Proteolysis of HCF-1. *Cell* **144**:
438 376–388.

439 Chao L, Yang S, Li H, Long C, Xi Q, Zuo Y. 2022. Competitive binding of TET1 and
440 DNMT3A/B cooperates the DNA methylation pattern in human embryonic stem cells.
441 *Biochim Biophys Acta (BBA) - Gene Regul Mech* **1865**: 194861.

442 Chotalia M, Smallwood SA, Ruf N, Dawson C, Lucifero D, Frontera M, James K, Dean W,
443 Kelsey G. 2009. Transcription is required for establishment of germline methylation marks at
444 imprinted genes. *Genes Dev* **23**: 105–117.
445 http://genesdev.cshlp.org/cgi/doi/10.1101/gad.495809.

446 Chrysanthou S, Tang Q, Lee J, Taylor SJ, Zhao Y, Steidl U, Zheng D, Dawlaty MM. 2022. The
447 DNA dioxygenase Tet1 regulates H3K27 modification and embryonic stem cell biology
448 independent of its catalytic activity. *Nucleic Acids Res* **50**: 3169–3189.

449 Dawlaty MM, Breiling A, Le T, Raddatz G, Barrasa MI, Cheng AW, Gao Q, Powell BE, Li Z,
450 Xu M, et al. 2013. Combined deficiency of Tet1 and Tet2 causes epigenetic abnormalities but
451 is compatible with postnatal development. *Dev Cell* **24**: 310–323.
452 http://linkinghub.elsevier.com/retrieve/pii/S1534580712005898.

453 Deplus R, Delatte B, Schwinn MK, Defrance M, Méndez J, Murphy N, Dawson MA, Volkmar
454 M, Putmans P, Calonne E, et al. 2013. TET2 and TET3 regulate GlcNAcylation and H3K4
455 methylation through OGT and SET1/COMPASS. *EMBO J* **32**: 645–655.
456 http://emboj.embopress.org/cgi/doi/10.1038/emboj.2012.357.

457 Dhayalan A, Rajavelu A, Rathert P, Tamas R, Jurkowska RZ, Ragozin S, Jeltsch A. 2010. The
458 Dnmt3a PWWP Domain Reads Histone 3 Lysine 36 Trimethylation and Guides DNA
459 Methylation*. *J Biol Chem* **285**: 26114–26120.

460 Dura M, Teissandier A, Armand M, Barau J, Lapoujade C, Fouchet P, Bonneville L, Schulz M,
461 Weber M, Baudrin LG, et al. 2022. DNMT3A-dependent DNA methylation is required for
462 spermatogonial stem cells to commit to spermatogenesis. *Nat Genet* **54**: 469–480.

463 Erkek S, Hisano M, Liang C-Y, Gill M, Murr R, Dieker J, Schübeler D, Vlag J van der, Stadler
464 MB, Peters AHFM. 2013. Molecular determinants of nucleosome retention at CpG-rich
465 sequences in mouse spermatozoa. *Nat Struct Mol Biol* **20**: 868–875.

466 Ernst J, Kellis M. 2017. Chromatin-state discovery and genome annotation with ChromHMM.
467 *Nat Protoc* **12**: 2478–2492.

468 Ernst J, Kellis M. 2012. ChromHMM: automating chromatin-state discovery and
469 characterization. *Nat Methods* **9**: 215–216.

470 Fanourgakis G, Gaspa-Toneu L, Komarov PA, Papasaikas P, Ozonov EA, Smallwood SA, Peters
471 AHFM. 2025. DNA methylation modulates nucleosome retention in sperm and H3K4
472 methylation deposition in early mouse embryos. *Nat Commun* **16**: 465.

473 Gel B, Díez-Villanueva A, Serra E, Buschbeck M, Peinado MA, Malinverni R. 2015. regioneR:
474 an R/Bioconductor package for the association analysis of genomic regions based on
475 permutation tests. *Bioinformatics* **32**: 289–291.

476 Goodman RH, Smolik S. 2000. CBP/p300 in cell growth, transformation, and development.
477 *Genes Dev* **14**: 1553–1577.

478 Gu T, Lin X, Cullen SM, Luo M, Jeong M, Estecio M, Shen J, Hardikar S, Sun D, Su J, et al.
479 2018. DNMT3A and TET1 cooperate to regulate promoter epigenetic landscapes in mouse
480 embryonic stem cells. *Genome Biol* **19**: 88.
481 https://genomebiology.biomedcentral.com/articles/10.1186/s13059-018-1464-7.

482 Guenther MG, Levine SS, Boyer LA, Jaenisch R, Young RA. 2007. A chromatin landmark and
483 transcription initiation at most promoters in human cells. *Cell* **130**: 77–88.

484 Hajkova P, Ancelin K, Waldmann T, Lacoste N, Lange UC, Cesari F, Lee C, Almouzni G,
485 Schneider R, Surani MA. 2008. Chromatin dynamics during epigenetic reprogramming in the
486 mouse germ line. *Nature* **452**: 877–881.
487 http://www.nature.com/doifinder/10.1038/nature06714.

488 Hajkova P, Erhardt S, Lane N, Haaf T, El-Maarri O, Reik W, Walter J, Surani MA. 2002.
489 Epigenetic reprogramming in mouse primordial germ cells. *Mech Dev* **117**: 15–23.
490 http://eutils.ncbi.nlm.nih.gov/entrez/eutils/elink.fcgi?dbfrom=pubmed&id=12204247&retmo
491 de=ref&cmd=prlinks.

492 Hanna CW, Taudt A, Huang J, Gahurova L, Kranz A, Andrews S, Dean W, Stewart AF,
493 Colomé-Tatché M, Kelsey G. 2018. MLL2 conveys transcription-independent H3K4
494 trimethylation in oocytes. *Nat Struct Mol Biol* **25**: 73–82.
495 http://www.nature.com/articles/s41594-017-0013-5.

496 Hill PWS, Leitch HG, Requena CE, Sun Z, Amouroux R, Roman-Trufero M, Borkowska M,
497 Terragni J, Vaisvila R, Linnett S, et al. 2018. Epigenetic reprogramming enables the transition
498 from primordial germ cell to gonocyte. *Nature* **555**: 392–396.
499 http://www.nature.com/doifinder/10.1038/nature25964.

500 Huang G, Liu L, Wang H, Gou M, Gong P, Tian C, Deng W, Yang J, Zhou T-T, Xu G-L, et al.
501 2020. Tet1 Deficiency Leads to Premature Reproductive Aging by Reducing Spermatogonia
502 Stem Cells and Germ Cell Differentiation. *iScience* **23**: 100908.

503 Huang Y, Sitwala K, Bronstein J, Sanders D, Dandekar M, Collins C, Robertson G, MacDonald
504 J, Cezard T, Bilenky M, et al. 2012. Identification and characterization of Hoxa9 binding sites
505 in hematopoietic cells. *Blood* **119**: 388–398.

506 Ito S, Shen L, Dai Q, Wu SC, Collins LB, Swenberg JA, He C, Zhang Y. 2011. Tet Proteins Can
507 Convert 5-Methylcytosine to 5-Formylcytosine and 5-Carboxylcytosine. *Science* **333**: 1300–
508 1303.

509 Joshi K, Liu S, S.J. PB, Zhang J. 2022. Mechanisms that regulate the activities of TET proteins.
510 *Cell Mol Life Sci* **79**: 363.

511 Kaneda M, Okano M, Hata K, Sado T, Tsujimoto N, Li E, Sasaki H. 2004. Essential role for de
512 novo DNA methyltransferase Dnmt3a in paternal and maternal imprinting. *Nature* **429**: 900–
513 903.

514 Kato Y, Kaneda M, Hata K, Kumaki K, Hisano M, Kohara Y, Okano M, Li E, Nozaki M, Sasaki
515 H. 2007. Role of the Dnmt3 family in de novo methylation of imprinted and repetitive
516 sequences during male germ cell development in the mouse. *Hum Mol Genet* **16**: 2272–2280.
517 https://academic.oup.com/hmg/article-lookup/doi/10.1093/hmg/ddm179.

518 Ko M, Bandukwala HS, An J, Lamperti ED, Thompson EC, Hastie R, Tsangaratou A, Rajewsky
519 K, Koralov SB, Rao A. 2011. Ten-Eleven-Translocation 2 (TET2) negatively regulates
520 homeostasis and differentiation of hematopoietic stem cells in mice. *Proc Natl Acad Sci USA*
521 **108**: 14566–14571. http://www.pnas.org/cgi/doi/10.1073/pnas.1112317108.

522 Kobayashi H, Sakurai T, Imai M, Takahashi N, Fukuda A, Yayoi O, Sato S, Nakabayashi K,
523 Hata K, Sotomaru Y, et al. 2012. Contribution of intragenic DNA methylation in mouse
524 gametic DNA methylomes to establish oocyte-specific heritable marks. ed. W. Reik. *PLoS*
525 *Genet* **8**: e1002440. https://dx.plos.org/10.1371/journal.pgen.1002440.

526 Kobayashi H, Sakurai T, Miura F, Imai M, Mochiduki K, Yanagisawa E, Sakashita A, Wakai T,
527 Suzuki Y, Ito T, et al. 2013. High-resolution DNA methylome analysis of primordial germ

528 cells identifies gender-specific reprogramming in mice. *Genome Res* **23**: 616–627.
529 http://genome.cshlp.org/cgi/doi/10.1101/gr.148023.112.

530 Kohli RM, Zhang Y. 2013. TET enzymes, TDG and the dynamics of DNA demethylation.
531 *Nature* **502**: 472–479. http://www.nature.com/doifinder/10.1038/nature12750.

532 Lauberth SM, Nakayama T, Wu X, Ferris AL, Tang Z, Hughes SH, Roeder RG. 2013. H3K4me3
533 Interactions with TAF3 Regulate Preinitiation Complex Assembly and Selective Gene
534 Activation. *Cell* **152**: 1021–1036.

535 Lee SM, Loo CE, Prasasya RD, Bartolomei MS, Kohli RM, Zhou W. 2024. Low-input and
536 single-cell methods for Infinium DNA methylation BeadChips. *Nucleic Acids Res* **52**: e38–
537 e38.

538 Lengner CJ, Camargo FD, Hochedlinger K, Welstead GG, Zaidi S, Gokhale S, Scholer HR,
539 Tomilin A, Jaenisch R. 2007. Oct4 expression is not required for mouse somatic stem cell
540 self-renewal. *Cell Stem Cell* **1**: 403–415.
541 https://linkinghub.elsevier.com/retrieve/pii/S1934590907000859.

542 Lian H, Li W-B, Jin W-L. 2016. The emerging insights into catalytic or non-catalytic roles of
543 TET proteins in tumors and neural development. *Oncotarget* **7**: 64512–64525.

544 Maezawa S, Sakashita A, Yukawa M, Chen X, Takahashi K, Alavattam KG, Nakata I, Weirauch
545 MT, Barski A, Namekawa SH. 2020. Super-enhancer switching drives a burst in gene
546 expression at the mitosis-to-meiosis transition. *Nat Struct Mol Biol* **27**: 978–988.

547 Molaro A, Hodges E, Fang F, Song Q, McCombie WR, Hannon GJ, Smith AD. 2011. Sperm
548 Methylation Profiles Reveal Features of Epigenetic Inheritance and Evolution in Primates.
549 *Cell* **146**: 1029–1041.

550 Ooi SKT, Qiu C, Bernstein E, Li K, Jia D, Yang Z, Erdjument-Bromage H, Tempst P, Lin S-P,
551 Allis CD, et al. 2007. DNMT3L connects unmethylated lysine 4 of histone H3 to de novo
552 methylation of DNA. *Nature* **448**: 714–717. http://www.nature.com/articles/nature05987.

553 Prasasya RD, Caldwell BA, Liu Z, Wu S, Leu NA, Fowler JM, Cincotta SA, Laird DJ, Kohli
554 RM, Bartolomei MS. 2024. Iterative oxidation by TET1 is required for reprogramming of
555 imprinting control regions and patterning of mouse sperm hypomethylated regions. *Dev Cell*
556 **59**: 1010-1027.e8.

557 Saitou M, Kagiwada S, Kurimoto K. 2011. Epigenetic reprogramming in mouse pre-implantation
558 development and primordial germ cells. *Development* **139**: 15–31.

559 Saitou M, Payer B, O'Carroll D, Ohinata Y, Surani MA. 2005. Blimp1 and the Emergence of the
560 Germ Line during Development in the Mouse. *Cell Cycle* **4**: 1736–1740.

561 SanMiguel JM, Abramowitz LK, Bartolomei MS. 2018. Imprinted gene dysregulation in a Tet1
562 null mouse model is stochastic and variable in the germline and offspring. *Development* **145**:
563 dev160622. http://dev.biologists.org/lookup/doi/10.1242/dev.160622.

564 Schneider R, Bannister AJ, Myers FA, Thorne AW, Crane-Robinson C, Kouzarides T. 2004.
565 Histone H3 lysine 4 methylation patterns in higher eukaryotic genes. *Nat Cell Biol* **6**: 73–77.

566 Seisenberger S, Andrews S, Krueger F, Arand J, Walter J, Santos F, Popp C, Thienpont B, Dean
567 W, Reik W. 2012. The dynamics of genome-wide DNA methylation reprogramming in mouse
568 primordial germ cells. *Mol Cell* **48**: 849–862.
569 http://linkinghub.elsevier.com/retrieve/pii/S109727651200932X.

570 Shirane K, Lorincz M. 2023. Epigenetic Mechanisms Governing Female and Male Germline
571 Development in Mammals. *Sex Dev* **16**: 365–387.

572 Shirane K, Miura F, Ito T, Lorincz MC. 2020. NSD1-deposited H3K36me2 directs de novo
573 methylation in the mouse male germline and counteracts Polycomb-associated silencing. *Nat*
574 *Genet* **52**: 1088–1098.

575 Singh P, Li AX, Tran DA, Oates N, Kang E-R, Wu X, Szabó PE. 2013. De novo DNA
576 methylation in the male germ line occurs by default but is excluded at sites of H3K4
577 methylation. *Cell Rep* **4**: 205–219.
578 https://linkinghub.elsevier.com/retrieve/pii/S2211124713002805.

579 Smith ZD, Meissner A. 2013. DNA methylation: roles in mammalian development. *Nat Rev*
580 *Genet* **14**: 204–220.

581 Song C-X, Szulwach KE, Fu Y, Dai Q, Yi C, Li X, Li Y, Chen C-H, Zhang W, Jian X, et al.
582 2011. Selective chemical labeling reveals the genome-wide distribution of 5-
583 hydroxymethylcytosine. *Nat Biotechnol* **29**: 68–72.

584 Stephens DC, Poon GMK. 2016. Differential sensitivity to methylated DNA by ETS-family
585 transcription factors is intrinsically encoded in their DNA-binding domains. *Nucleic Acids*
586 *Res* **44**: 8671–8681.

587 Stewart KR, Veselovska L, Kelsey G. 2016. Establishment and functions of DNA methylation in
588 the germline. *Epigenomics* **8**: 1399–1413. https://www.futuremedicine.com/doi/10.2217/epi-
589 2016-0056.

590 Stewart KR, Veselovska L, Kim J, Huang J, Saadeh H, Tomizawa S-I, Smallwood SA, Chen T,
591 Kelsey G. 2015. Dynamic changes in histone modifications precede de novo DNA
592 methylation in oocytes. *Genes Dev* **29**: 2449–2462.
593 http://genesdev.cshlp.org/lookup/doi/10.1101/gad.271353.115.

594 Vella P, Scelfo A, Jammula S, Chiacchiera F, Williams K, Cuomo A, Roberto A, Christensen J,
595 Bonaldi T, Helin K, et al. 2013. Tet proteins connect the O-linked N-acetylglucosamine

596 transferase Ogt to chromatin in embryonic stem cells. *Mol Cell* **49**: 645–656.
597 https://linkinghub.elsevier.com/retrieve/pii/S1097276512010556.

598 Wang H, Fan Z, Shliaha PV, Miele M, Hendrickson RC, Jiang X, Helin K. 2023. H3K4me3
599 regulates RNA polymerase II promoter-proximal pause-release. *Nature* **615**: 339–348.

600 Williams K, Christensen J, Pedersen MT, Johansen JV, Cloos PAC, Rappsilber J, Helin K. 2011.
601 TET1 and hydroxymethylcytosine in transcription and DNA methylation fidelity. *Nature* **473**:
602 343–348. http://www.nature.com/articles/nature10066.

603 Wu H, D'Alessio AC, Ito S, Xia K, Wang Z, Cui K, Zhao K, Sun YE, Zhang Y. 2011. Dual
604 functions of Tet1 in transcriptional regulation in mouse embryonic stem cells. *Nature* **473**:
605 389–393. http://www.nature.com/articles/nature09934.

606 Xia B, Yan Y, Baron M, Wagner F, Barkley D, Chiodin M, Kim SY, Keefe DL, Alukal JP,
607 Boeke JD, et al. 2020. Widespread Transcriptional Scanning in the Testis Modulates Gene
608 Evolution Rates. *Cell* **180**: 248-262.e21.

609 Yamaguchi S, Hong K, Liu R, Shen L, Inoue A, Diep D, Zhang K, Zhang Y. 2012. Tet1 controls
610 meiosis by regulating meiotic gene expression. *Nature* **492**: 443–447.
611 http://www.nature.com/articles/nature11709.

612 Yamaguchi S, Shen L, Liu Y, Sendler D, Zhang Y. 2013. Role of Tet1 in erasure of genomic
613 imprinting. *Nature* **504**: 460–464. http://www.nature.com/articles/nature12805.

614 Yan R, Cheng X, Gu C, Xu Y, Long X, Zhai J, Sun F, Qian J, Du Y, Wang H, et al. 2022.
615 Dynamics of DNA hydroxymethylation and methylation during mouse embryonic and
616 germline development. *Nat Genet* 1–14.

617 Yang C, Shapiro LH, Rivera M, Kumar A, Brindle PK. 1998. A Role for CREB Binding Protein
618 and p300 Transcriptional Coactivators in Ets-1 Transactivation Functions. *Mol Cell Biol* **18**:
619 2218–2229.

620 Zhang T, Murphy MW, Gearhart MD, Bardwell VJ, Zarkower D. 2014. The mammalian
621 Doublesex homolog DMRT6 coordinates the transition between mitotic and meiotic
622 developmental programs during spermatogenesis. *Development* **141**: 3662–3671.

623 Zhang Y, Jurkowska R, Soeroes S, Rajavelu A, Dhayalan A, Bock I, Rathert P, Brandt O,
624 Reinhardt R, Fischle W, et al. 2010. Chromatin methylation activity of Dnmt3a and
625 Dnmt3a/3L is guided by interaction of the ADD domain with the histone H3 tail. *Nucleic*
626 *Acids Res* **38**: 4246–4253.

627 Zhao J, Lu P, Wan C, Huang Y, Cui M, Yang X, Hu Y, Zheng Y, Dong J, Wang M, et al. 2021.
628 Cell-fate transition and determination analysis of mouse male germ cells throughout
629 development. *Nat Commun* **12**: 6839.

630 Zhu F, Zhu Q, Ye D, Zhang Q, Yang Y, Guo X, Liu Z, Jiapaer Z, Wan X, Wang G, et al. 2018.
631 Sin3a–Tet1 interaction activates gene transcription and is required for embryonic stem cell
632 pluripotency. *Nucleic Acids Res* **46**: 6026–6040.

633

634

635

636 **Figure legends**

637 **Figure 1. The majority of methylation defects in *Tet1*$^{-/-}$ sperm do not result from**

638 **incomplete methylation erasure during epigenetic reprogramming.**

639 A) Top enriched design groups based on the Illumina Infinium Mouse Methylation BeadChip

640 manifest for hypermethylated DMRs in *Tet1*$^{-/-}$ PGCs.

641 B) Heatmap of probes associated with the most enriched GO term among hypermethylated

642 DMRs in *Tet1*$^{-/-}$ PGCs.

643 C) Scatterplot showing overlap between hypermethylated DMRs and DEGs in *Tet1*$^{-/-}$ PGCs.

644 D) Comparison of hypermethylated probes (differentially methylated regions, DMRs: FDR ≤

645 0.05; >10% methylation difference) in E13.5 *Tet1*$^{-/-}$ PGCs (n=8) vs *Tet1*$^{+/+}$ (WT, n=8) and those

646 previously reported in *Tet1*$^{-/-}$ sperm (Prasasya et al. 2024).

647 E) Methylation levels in E13.5 PGCs (top) or sperm (bottom) for *Tet1*$^{-/-}$ (black) and *Tet1*$^{+/+}$ (blue).

648 DMRs are subsetted by origin of hypermethylation (i–iv). Average methylation levels are

649 denoted by dotted vertical lines.

650

651 **Figure 2. Abnormal de novo methylation acquisition is associated with H3K4me3 erosion**

652 **in *Tet1*$^{-/-}$ male germ cells.**

653 A) Metaplot of H3K4me3 signals over genic regions (top) or consensus intergenic peaks

654 (bottom).

655 B) Distribution of H3K4me3 peaks overlapping sperm HMRs compared to non-HMRs (**** $p <$

656 0.0001, Fisher's exact test).

657 C) Scatterplot of *Tet1*$^{-/-}$ sperm DMRs and regions with differential H3K4me3 in *Tet1*$^{-/-}$

658 prospermatogonia. H3K4me3 peaks overlapping with DMRs in *Tet1*$^{-/-}$ sperm are highlighted in

659 black circles. Fisher's exact test for hypermethylated DMRs overlapping H3K4me3-depleted vs

660 other regions.

661 D) (Top) Metagene plots of H3K4me3 signals in *Tet1*$^{-/-}$ and *Tet1*$^{+/+}$ prospermatogonia
662 overlapping subsets of *Tet1*$^{-/-}$ sperm hypermethylated DMRs (hypermorphic gain, ectopic gain,
663 incomplete erasure) or *Tet1*$^{-/-}$ PGC hypermethylated DMRs. (Bottom) Boxplots of mean
664 H3K4me3 signals over 1 kb windows centered on subsets of hypermethylated DMRs (**** $p <$
665 0.0001, Wilcoxon signed-rank test).
666 E) Genome browser tracks for representative sperm hypermethylated DMRs from abnormal de
667 novo methylation at genic region (left) or intergenic region (middle). *Nespas* is a representative
668 ICR that is hypermethylated due to incomplete erasure (right).
669
670 **Figure 3. H3K4me3 enrichment in prospermatogonia may regulate later stages of**
671 **spermatogenesis**
672 A) Scatter plot of significantly altered H3K4me3 peaks in *Tet1*$^{-/-}$ prospermatogonia (vs WT) at
673 gene promoters and their associated gene expression changes as measured by total RNA-seq.
674 Differentially expressed transcripts (FDR ≤ 0.05, ≥2-fold change) are highlighted with blue
675 (downregulated) or red (upregulated) dots.
676 B) Enrichment of H3K4me3 peaks lost or gained in *Tet1*$^{-/-}$ prospermatogonia across chromatin
677 states during spermatogenesis (SSC: spermatogonial stem cells; SPG: spermatogonia; PS:
678 pachytene spermatocyte; RS: round spermatid), using ChromHMM. Chromatin states
679 assignment is based on the ENCODE consortium projects and are defined in Supplemental Fig.
680 S3D (Ernst and Kellis 2017) . Scale bar indicates fold enrichment.
681 C) Motif enrichment for regions with H3K4me3 loss after masking repetitive elements.
682 D) Motif enrichment for regions with H3K4me3 gain.
683
684 **Figure 4. The non-catalytic, full length TET1^{HxD} reverts most H3K4me3 changes in *Tet1*$^{-/-}$**
685 **prospermatogonia to WT levels.**

686 A) Alluvial plot of differentially enriched H3K4me3 peaks in *Tet1*$^{-/-}$ vs *Tet1*$^{+/+}$ and their status in
687 *Tet1*$^{HxD/HxD}$ vs *Tet1*$^{+/+}$. Light brown ribbons indicate peaks altered in *Tet1*$^{-/-}$ but not in *Tet1*$^{HxD/HxD}$.
688 B) Scatterplot of *Tet1*$^{HxD/HxD}$ sperm DMRs and regions with differential H3K4me3 in *Tet1*$^{HxD/HxD}$
689 prospermatogonia. H3K4me3 peaks overlapping with DMRs in *Tet1*$^{HxD/HxD}$ sperm are highlighted
690 in brown circles. Fisher's exact test for hypermethylated DMRs overlapping H3K4me3-depleted
691 vs other regions.
692 C) Proportion of regions with H3K4me3 loss in Tet1 mutants that overlap hypermethylated
693 sperm DMRs; two-sample proportion test.
694 D) Boxplots of median H3K4me3 signals over 1 kb windows centered on of DMRs that were
695 significantly hypermethylated in *Tet1*$^{-/-}$ sperm but were not hypermethylated in *Tet1*$^{HxD/HxD}$ sperm
696 (left, rescued DMRs) or stayed hypermethylated in *Tet1*$^{HxD/HxD}$ sperm (right, not-rescued DMRs)
697 (Prasasya et al. 2024) (**** $p < 0.0001$, Wilcoxon signed-rank test).
698 E) Fold change of H3K4me3 signals in *Tet1*$^{-/-}$ compared to *Tet1*$^{+/+}$ calculated across two subsets
699 of sperm DMRs defined in D (**** $p < 0.0001$, Wilcoxon signed-rank test).
700 F) Boxplots of median H3K4me3 signals over 1 kb windows centered on hypermethylated
701 DMRs defined in D in *Tet1*$^{-/-}$ prospermatogonia (Wilcoxon signed-rank test; not-significant).
702 G) Fold change of H3K4me3 signals in *Tet1*$^{HxD/HxD}$ compared to *Tet1*$^{-/-}$ calculated across two
703 subsets of sperm DMRs defined in D (**** $p < 0.0001$, Wilcoxon signed-rank test).
704 H) Ridgeline plots showing the relative frequency distribution of rescued and not-rescued DMRs
705 and the associated H3K4me3 signals found in *Tet1*$^{+/+}$, *Tet1*$^{-/-}$, or *Tet1*$^{HxD/HxD}$ prospermatogonia.
706 The median H3K4me3 signal for each genotype across the two subsets of sperm DMRs is
707 indicated with vertical dashed lines of matched colors (blue: *Tet1*$^{+/+}$, black: *Tet1*$^{-/-}$, or brown:
708 *Tet1*$^{HxD/HxD}$).
709 I) The strength of overlap between distinct subsets of DMRs (rescued in *Tet1*$^{HxD/HxD}$ sperm or
710 not-rescued in *Tet1*$^{HxD/HxD}$ sperm) and regions where H3K4me3 was reverted to WT levels in
711 *Tet1*$^{HxD/HxD}$ prospermatogonia following observed depletion in *Tet1*$^{-/-}$ prospermatogonia as

712 determined by permutation test (Z-score from 1000 permutations of randomly selected regions
713 consistent with Illumina Bead Chip array coverage).
714 J) Schematic diagram depicting differential responsiveness in the relative levels of H3K4me3
715 depletion in response to the loss of TET1 (*Tet1*$^{-/-}$, black, compared to *Tet1*$^{+/+}$, blue). This
716 depletion correlates with aberrant methylation acquisition, resulting in hypermethylated DMRs in
717 *Tet1*$^{-/-}$ sperm. Catalytically inactive TET1^{HxD} enhances H3K4me3 deposition in
718 prospermatogonia toward WT levels. However, not all restoration of H3K4me3 is associated
719 with rescue of abnormal methylation. It is plausible that additional chromatin features, beyond
720 H3K4me3, may contribute to differential susceptibility to aberrant *de novo* methylation at the two
721 DMR subsets.

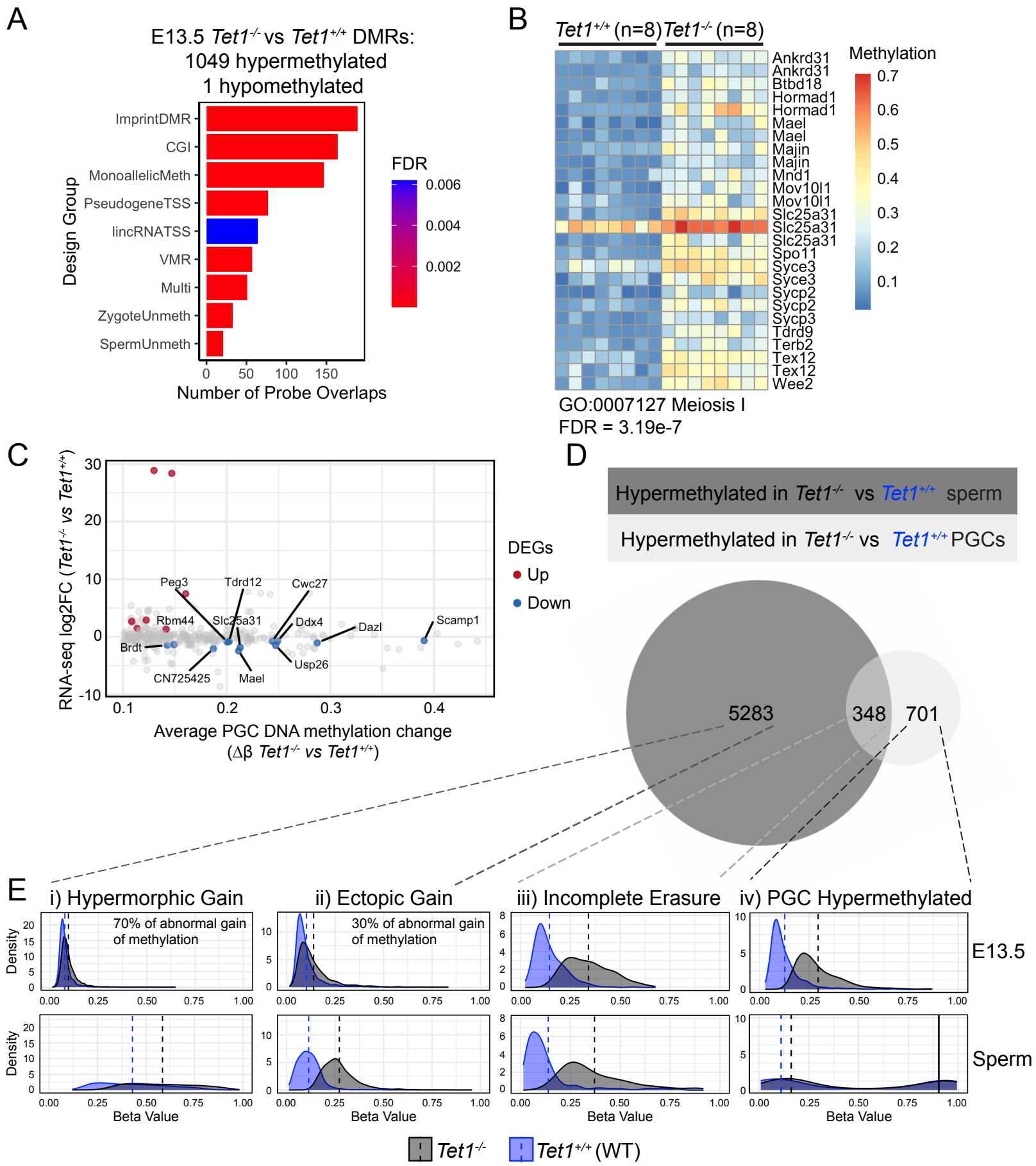
A
E13.5 Tet1-/- vs Tet1+/+ DMRs:
1049 hypermethylated
1 hypomethylated
ImprintDMR
CGI
MonoallelicMeth
PseudogeneTSS
lincRNATSS
VMR
Multi
ZygoteUnmeth
SpermUnmeth
Design Group
Number of Probe Overlaps
FDR
0.006
0.004
0.002
B
Tet1+/+ (n=8)
Tet1-/- (n=8)
Ankrd31
Ankrd31
Btbd18
Hormad1
Hormad1
Mael
Mael
Majin
Majin
Mnd1
Mov10l1
Mov10l1
Slc25a31
Slc25a31
Slc25a31
Spo11
Syce3
Syce3
Sycp2
Sycp2
Sycp3
Tdrd9
Terb2
Tex12
Tex12
Wee2
Methylation
GO:0007127 Meiosis I
FDR = 3.19e-7
C
RNA-seq log2FC (Tet1-/- vs Tet1+/+)
Average PGC DNA methylation change
(Δβ Tet1-/- vs Tet1+/+)
Peg3
Tdrd12
Cwc27
Rbm44
Slc25a31
Ddx4
Dazl
Scamp1
Brdt
Usp26
CN725425
Mael
DEGs
Up
Down
D
Hypermethylated in Tet1-/- vs Tet1+/+ sperm
Hypermethylated in Tet1-/- vs Tet1+/+ PGCs
5283
348
701
E
i) Hypermorphic Gain
ii) Ectopic Gain
iii) Incomplete Erasure
iv) PGC Hypermethylated
70% of abnormal gain of methylation
30% of abnormal gain of methylation
E13.5
Sperm
Density
Beta Value
Tet1-/-
Tet1+/+ (WT)

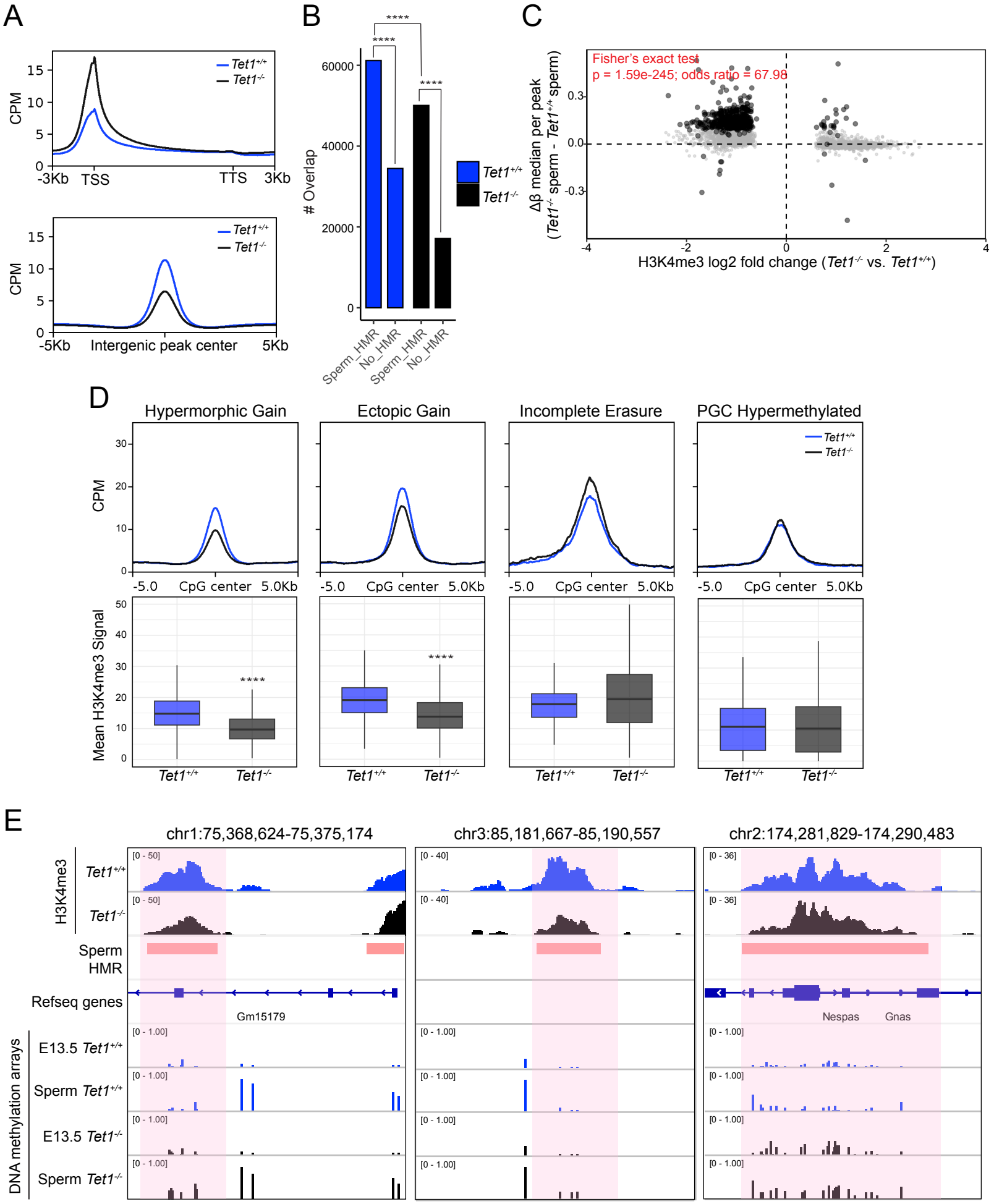
A
CPM
Tet1+/+
Tet1-/-
-3Kb TSS TTS 3Kb
-5Kb Intergenic peak center 5Kb
B
Overlap
****
Sperm_HMR
No_HMR
C
Fisher's exact test
p = 1.59e-245; odds ratio = 67.98
Δβ median per peak (Tet1-/- sperm - Tet1+/+ sperm)
H3K4me3 log2 fold change (Tet1-/- vs. Tet1+/+)
D
Hypermorphic Gain
Ectopic Gain
Incomplete Erasure
PGC Hypermethylated
CpG center
Mean H3K4me3 Signal
E
chr1:75,368,624-75,375,174
chr3:85,181,667-85,190,557
chr2:174,281,829-174,290,483
H3K4me3
Sperm HMR
Refseq genes
Gm15179
Nespas
Gnas
DNA methylation arrays
E13.5 Tet1+/+
Sperm Tet1+/+
E13.5 Tet1-/-
Sperm Tet1-/-

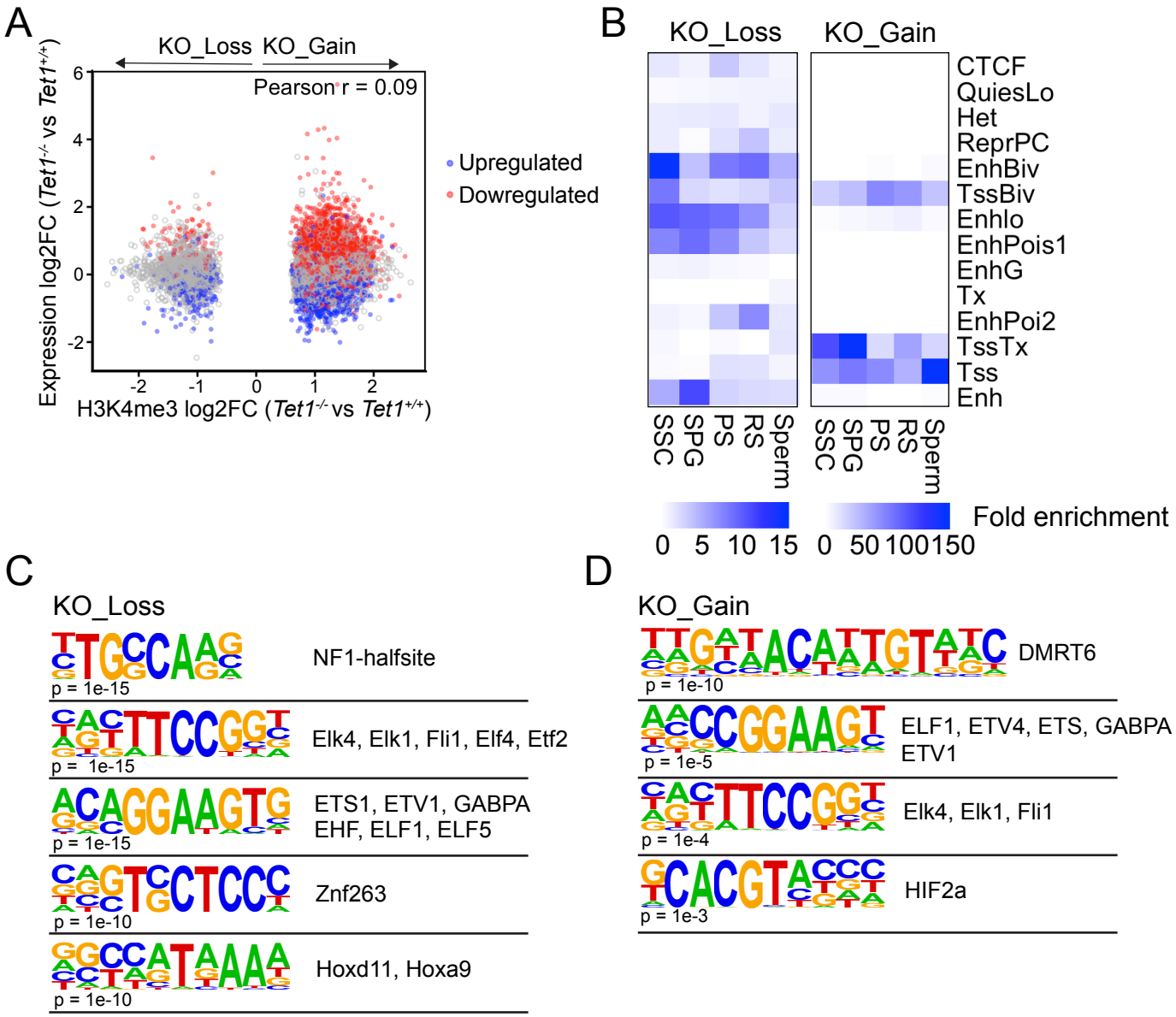
A
KO_Loss
KO_Gain
Pearson r = 0.09
Upregulated
Dowregulated
Expression log2FC (Tet1-/- vs Tet1+/+)
H3K4me3 log2FC (Tet1-/- vs Tet1+/+)
B
KO_Loss
KO_Gain
CTCF
QuiesLo
Het
ReprPC
EnhBiv
TssBiv
Enhlo
EnhPois1
EnhG
Tx
EnhPoi2
TssTx
Tss
Enh
SSC
SPG
PS
RS
Sperm
Fold enrichment
0 5 10 15
0 50 100 150
C
KO_Loss
p = 1e-15
NF1-halfsite
p = 1e-15
Elk4, Elk1, Fli1, Elf4, Etf2
p = 1e-15
ETS1, ETV1, GABPA
EHF, ELF1, ELF5
p = 1e-10
Znf263
p = 1e-10
Hoxd11, Hoxa9
D
KO_Gain
p = 1e-10
DMRT6
p = 1e-5
ELF1, ETV4, ETS, GABPA
ETV1
p = 1e-4
Elk4, Elk1, Fli1
p = 1e-3
HIF2a

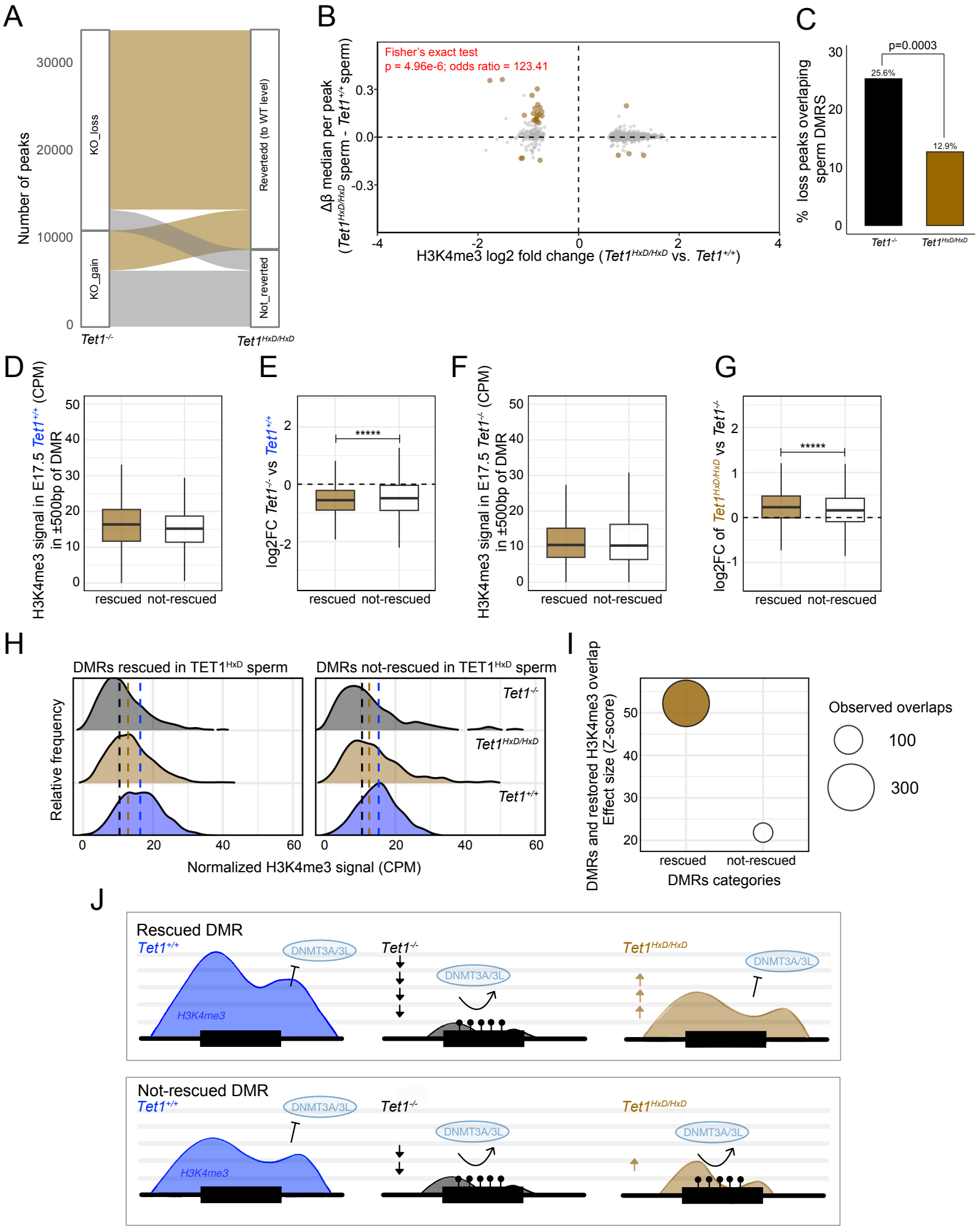
A
Number of peaks
30000
20000
10000
0
KO_loss
KO_gain
Reverted (to WT level)
Not_reverted
Tet1-/-
Tet1HxD/HxD
B
Fisher's exact test
p = 4.96e-6; odds ratio = 123.41
Δβ median per peak
(Tet1HxD/HxD sperm - Tet1+/+ sperm)
0.3
0.0
-0.3
-4
-2
0
2
4
H3K4me3 log2 fold change (Tet1HxD/HxD vs. Tet1+/+)
C
p=0.0003
% loss peaks overlaping sperm DMRS
25.6%
12.9%
30
20
10
0
Tet1-/-
Tet1HxD/HxD
D
H3K4me3 signal in E17.5 Tet1+/+ (CPM) in ±500bp of DMR
50
40
30
20
10
0
rescued
not-rescued
E
log2FC Tet1-/- vs Tet1+/+
*****
2
0
-2
rescued
not-rescued
F
H3K4me3 signal in E17.5 Tet1-/- (CPM) in ±500bp of DMR
50
40
30
20
10
0
rescued
not-rescued
G
log2FC of Tet1HxD/HxD vs Tet1-/-
*****
2
1
0
-1
rescued
not-rescued
H
DMRs rescued in TET1HxD sperm
DMRs not-rescued in TET1HxD sperm
Relative frequency
Tet1-/-
Tet1HxD/HxD
Tet1+/+
0
20
40
60
Normalized H3K4me3 signal (CPM)
I
DMRs and restored H3K4me3 overlap
Effect size (Z-score)
50
40
30
20
rescued
not-rescued
DMRs categories
Observed overlaps
100
300
J
Rescued DMR
Tet1+/+
DNMT3A/3L
H3K4me3
Tet1-/-
DNMT3A/3L
Tet1HxD/HxD
DNMT3A/3L
Not-rescued DMR
Tet1+/+
DNMT3A/3L
H3K4me3
Tet1-/-
DNMT3A/3L
Tet1HxD/HxD
DNMT3A/3L

Extended Methods

Genome-wide amplification of bisulfite mutagenized DNA

10 µL of bisulfite mutagenized (BSM) DNA eluted from EZ DNA methylation-Direct Kit (Zymo Research) was combined with 0.8 µL 10 mM dNTPs (BioRad, F560/170-8874), 4 µL 20 µM Random Primer 6 (NEB, S1230S), and nuclease-free water to a final volume of 16 µL. Samples were denatured at 98 °C for 1 min, rapidly cooled on ice for 2 min, then incubated at 37 °C for 30 min with 2 µL (10 U) of Klenow Fragment (3′→5′ exo–; NEB, M0212S) and 2 µL of the supplied buffer. A second round of Klenow amplification was done by denaturing samples for 98ºC for 1 min, followed by rapid cooling on ice. 2 µL of Klenow Fragment, 0.5 µL of supplied buffer, 0.8 µL of dNTPs, and 1.7 µL of water were added, followed by 37ºC incubation for 30 minutes. Reactions were heat-inactivated at 75 °C for 10 min and purified with SPRI beads (Beckman Coulter) at a 2× bead-to-sample volume ratio. Libraries were eluted in 11 µL nuclease-free water and DNA concentration was measured using Qubit High Sensitivity DNA Reagent (Invitrogen).

Libraries were denatured with 0.1 N NaOH immediately prior to hybridization onto the Infinium Mouse Methylation-12v1-0 BeadChip (Illumina). TECAN automation was used for sample loading onto the iScan System. Biological replicates for each genotype were as follows: E13.5, *Tet1*$^{+/+}$ (n = 8), *Tet1*$^{-/-}$ (n = 7).

CUT&RUN and Sequencing library preparation

CUT&RUN experiments were performed on samples of 4,000 nuclei isolated per epitope from cryopreserved germ cells as described above using CUTANA ChIC/CUT&RUN kit (EpiCypher). Cells were rapidly thawed and counted, followed by nuclei extraction using NE buffer (20 mM HEPES-KOH pH 7.9, 10mM KCl, 0.5 mM fresh spermidine, 0.1% Triton X-100, 20% glycerol plus protease inhibitors). Nuclei were bound to concanavalin A-coated magnetic beads pre-washed in cold bead activation buffer (EpiCypher) for 10 minutes at room temperature (RT). Nuclei were resuspended with H3K4me3 (1:100, Cell Signaling Technology antibody 2729) or IgG (1:50, CUTANA Rabbit IgG negative control antibody) in 50 µL of antibody binding buffer (CUTANA pre-wash buffer – 20 mM HEPES pH 7.5, 150 mM NaCl-, with 0.5 mM spermidine, 1x Roche complete protease inhibitor, 0.05% digitonin and 2mM EDTA) overnight at 4ºC. Samples were washed twice in cell permeabilization buffer (CUTANA pre-wash buffer with 0.5mM spermidine, 1x Roche complete protease inhibitor, and 0.05% digitonin) followed by incubation with pAG-MNase fusion protein for 1 hour at 4ºC. Cells were washed twice in cell permeabilization buffer, and 100mM $CaCl_2$ was added to activate cleavage for 1 hour at 4ºC. 2x CUTANA STOP buffer (170 mM NaCl, 20 mM EGTA, 0.05% digitonin, 50 µg/mL RNase A, 25µg/mL Glycogen) was added to quench the reaction. To release antibody-bound fragments, samples were incubated at 37 °C for 10 min, and the supernatant was isolated from the magnet-bound beads. 3 µL of 10% SDS and 2.5 µL of Proteinase K (20 mg/mL) were added to the samples (300 µL in 0.1x TE) and incubated at 70 °C for 10 min to digest residual proteins. DNA was extracted twice with phenol:chloroform with additional glycogen during DNA precipitation. Pellets were resuspended in 50 µL of Tris-EDTA buffer (1 mM Tris-HCl, pH 8; 0.1 mM EDTA).

CUT&RUN and 5hmC-Seal libraries were prepared using the NEBNext Ultra II DNA Library Prep Kit for Illumina with modifications. 1:25 fold dilution of Illumina adapter was used during adaptor ligation and libraries were amplified for 12–14 cycles using NEBNext Multiplex Oligos for Illumina Unique Dual Index Primer Pairs. Amplified libraries were cleaned using solid-phase reversible immobilization (SPRI) beads (Beckman Coulter), quantified using the Kapa library quantification kit for Illumina, and assessed for size distribution using the D5000 ScreenTape

Assay for TapeStation System (Agilent Technologies). Libraries were sequenced on Illumina NextSeq1000 instrument (60bpx60bp paired end).

RNA isolation

Snap-frozen cell pellets were directly transferred to 500 µL TRIzol Reagent (Invitrogen). Samples were incubated at RT for 10 min, followed by addition of 100 µL chloroform and incubation at RT for 3 min. Phase separation was performed by transferring mixture to MaXtract High Density tube (Qiagen) and centrifuging at maximum speed for 10 min at 4 °C. The aqueous phase was collected, mixed with 500 µL isopropanol and 2 µL of 2 mg/mL glycogen, and incubated at RT for 10 min to precipitate RNA. Samples were centrifuged at maximum speed for 10 min at 4 °C. The supernatant was discarded, and the RNA pellet was washed with 80% ethanol, briefly spun to eliminate residual ethanol, and air-dried for 5 min. RNA was resuspended in 17.5 µL TE buffer. To eliminate carry-over genomic DNA 2 µL Qiagen Buffer RDD and 0.5 µL Qiagen DNaseI were added and incubated at RT for 10 min. RNA was cleaned using 1.8× RNAClean XP Beads (Beckman Coulter) and RNA was eluted in 8 µL TE buffer.

Methylation array data analysis

Raw IDAT files were processed using SeSAMe R Package and the MM285 array manifest file to obtain methylation β-values with prep="I" (Zhou et al. 2018; Lee et al. 2024). Between-run batch correction was done using the R Package limma removeBatchEffect(). To determine differentially methylated probes, we included only CG probes with no NA values in all biological replicates. Batch-corrected β-values were converted into M-values (log2 ratio of methylated/unmethylated intensities). We then fit a linear model across conditions using the R package limma lmFit() function (Ritchie et al. 2015) . We applied eBayes() to moderate the per-locus variances and improved statistical power by borrowing information across loci. The contrast of interest (*Tet1*$^{-/-}$ vs *Tet1*$^{+/+}$ PGCs) was extracted and significance was determined using FDR (Benjamini-Hochberg) ≤ 0.05 and a minimum effect size of abs(delta.β) > 0.10. We used SeSAMe knowYourCG tool to test enrichments for probe design groups. A differentially methylated region (DMR) corresponds to each differentially methylated probe. Average β values (from biological replicates) of DMRs found in *Tet1*$^{-/-}$ PGCs and *Tet1*$^{-/-}$ sperm were used to create distribution plot to identify origin of hypermethylation.

Identification of sperm hypomethylated regions

Sperm hypomethylated regions (HMRs) were determined using hmr function of DNMTools, which uses hidden Markov model approach to identify methylation canyon in a supplied whole genome bisulfite sequencing methylation call data set (GSE56697: Wang et al. 2014).

ChromHMM model of methylation

The ChromHMM genome segmentation model was built using CTCF, Pol2, H3K4me1/2/3, H3K9me3, H3K27me3, H3K36me3, H3K9ac and H3K27ac datasets from spermatogonial stem cell (SSC), differentiated spermatogonia (SPG), pachytene spermatocytes (PS), round spermatids (RS), and sperm (GSE42629: Erkek et al. 2013; GSE158360: Chen et al. 2021; GSE79227: Jung et al. 2017; GSE89502: Maezawa et al. 2018; GSE207325: Pepin et al. 2024; GSE229246: Fanourgakis et al. 2025; GSE55471: Siklenka et al. 2015; GSE79227: Jung et al. 2017; GSE97778: Wang et al. 2018; GSE132446: Chen et al. 2020; GSE130652: Maezawa et al. 2020; GSE244675: Kitamura et al. 2023; GSE132054: Vara et al. 2019; GSE232398: Kang et al. 2025; GSE108717: Zuo et al. 2018; GSE153063: Yin et al. 2021; GSE49621: Hammoud et al. 2014; GSE137744: Liu et al. 2019; GSE132054: Vara et al. 2019; GSE44346: Margolin et al. 2014; GSE131656: Cheng et al. 2020). BAM files were binarized using the BinarizeBam function from ChromHMM with a Poisson threshold of 0.00001 and other default parameters.

State models with 4–16 states were built using the LearnModel function with default parameters. 14 states were selected for the final model. Chromatin state assignment is based on ENCODE consortium convention (Ernst and Kellis 2017).

RNAseq data analysis

Unique molecular index sequences were located in adaptor positions from raw reads using UMI-tools (Smith et al. 2017). UMI sequences were added to the read names and reads were quality-trimmed using Trim Galore (--phred 33 –clip_R2 6). Reads were aligned to mouse mm10 reference genome using STAR with default parameters and a maximum fragment size of 2000bp (Dobin et al. 2013). Reads with the same mapping coordinates and identical UMIs were collapsed to a single read.

Properly paired primary alignments were retained for downstream analysis using Samtools. Count matrices were generated using featureCounts against GENCODE annotation release M25 (Liao et al. 2014) . To remove lowly expressed genes prior to differential expression analysis, we applied library-size aware filtering using the R package edgeR filterByExpr() function. This approach retains genes with at least ~10 raw counts, scaled to each library's sequencing depth, in a sufficient number of replicates within at least one experimental group. For our libraries, this corresponded to CPM cutoffs ranging from ~0.5 to 0.8 across samples. Filtered count matrix were fed into the R package DESeq2 to perform normalization and differential expression analysis with FDR cut off ≤ 0.05 and minimum fold change of 2.

CUT&RUN and 5hmC-Seal data analysis

Raw reads were quality trimmed using Trim Galore (https://www.bioinformatics.babraham.ac.uk/projects/trim_galore/) using default parameters. Trimmed reads were aligned to mouse mm10 reference genome using Bowtie2 with parameters: –end-to-end –very-sensitive (Langmead and Salzberg 2012) . Following alignment, low quality reads (QMAP ≤ 10) and non-primary alignments were removed using SAMtools (view -q 10 -F 256) (Danecek et al. 2021) . Duplicated reads were removed using SAMtool rmdup with default parameters and mitochondrial reads were removed using grep function. Bigwig files normalized to count per million (CPM) were prepared using deepTools bamCoverage function with parameters: -bs 1 -normalizeUsing CPM (Ramírez et al. 2016). Peak calling was performed using Model-based Analysis of ChIP-seq (macs2; -qvalue 0.01, narrowPeak setting for CUT&RUN; broadPeak setting for 5hmC-Seal) against sample-matched IgG library as the background (Zhang et al. 2008). Peak sets and aligned reads were fed into the R Bioconductor package DiffBind where consensus peaks were determined based on the presence of peaks in at least two out of three biological replicates. DiffBind was used to perform normalization and differential enrichment analysis with FDR cut-off of ≤ 0.05 and minimum fold change of 1.5. Consensus or differentially enriched peaks were annotated for transcriptional start sites (TSS: -1kb to +100bp), exons, introns, transcriptional termination site (TTS: -100bp to +kb), or intergenic regions using HOMER annotatePeaks.pl function based on GENCODE annotation release M25 (Heinz et al. 2010).

For visualization, average bigwig files over the three replicates were created using bigwigCompare from deepTools. Metagene plots and heatmaps were generated using the computeMatrix, plotProfile, or plotHeatmap from deepTools with parameters reference point b-5000 a- 5000 for peak centers or -beforeRegionStartLength 3000 -afterRegionStartLength 3000 for genic regions. Overlap between H3K4me3 signals and *Tet1*$^{-/-}$ sperm differentially methylated regions (DMRs) of differing origins were identified using the R bioconductor package GenomicRanges findOverlaps function. Pairwise Wilcoxon rank sum test was used to compare average H3K4me3 signals across the overlap hits. Overlap between differentially enriched

H3K4me3 peaks in *Tet1*$^{-/-}$ prospermatogonia and all *Tet1*$^{-/-}$ sperm DMRs were identified using findOverlaps function. Fisher's exact test was used to test whether *Tet1*$^{-/-}$ sperm DMRs were significantly found within regions that lost H3K4me3. H3K4me3 fold changes of *Tet1*$^{-/-}$ vs WT or *Tet1*$^{HxD/HxD}$ vs WT were overlapped with TET1^{HxD}-rescued hypermethylated DMRs as defined in Prasasya et al. 2024 (FDR ≥ 0.05 in *Tet1*$^{HxD/HxD}$ vs WT; FDR ≤ 0.05, delta.beta > 0.10 in *Tet1*$^{-/-}$ vs WT). Pairwise Wilcoxon rank sum test with continuity correction was used to compare closeness to WT, which is calculated over fold change of H3K4me3 signals in *Tet1*$^{HxD/HxD}$ vs WT compared to *Tet1*$^{-/-}$ vs WT across rescued- or not-rescued DMRs.

To test the significance of overlaps between rescued or not-rescued subsets of DMRs with H3K4me3 regions that were restored in *Tet1*$^{HxD/HxD}$ compared to *Tet1*$^{-/-}$, we conducted 1000 permutations using R package regioneR. The test was implemented with permTest() using 1000 randomizations where at each iteration, the query regions were randomly shuffled across CpGs covered within the Illumina Bead Chip array while preserving their number and size distribution. For each randomized set, the overlap with the reference feature set was recalculated to generate a null distribution of expected overlaps. The empirical p-value was estimated as the proportion of permutations with equal or more extreme overlaps than observed.

R package ggplot2 was used to create box-and-whisker plots, distribution plots, scatter plots, dot plots, and alluvial plot. R package pheatmap was used to create heatmap. R package BioVenn was used to create venn diagrams.

Data availability

The accession number for raw and processed Illumina Mouse Infinium BeadChip, CUT&RUN, RNA-seq, and 5hmC-Seal data generated in this paper is submitted to GEO with the accession number GSE318256.

Reference

Chen Y, Lyu R, Rong B, Zheng Y, Lin Z, Dai R, Zhang X, Xie N, Wang S, Tang F, et al. 2020. Refined spatial temporal epigenomic profiling reveals intrinsic connection between PRDM9-mediated H3K4me3 and the fate of double-stranded breaks. *Cell Res* **30**: 256–268.

Chen Z, Djekidel MN, Zhang Y. 2021. Distinct dynamics and functions of H2AK119ub1 and H3K27me3 in mouse preimplantation embryos. *Nat Genet* **53**: 551–563.

Cheng K, Chen I-C, Cheng C-HE, Mutoji K, Hale BJ, Hermann BP, Geyer CB, Oatley JM, McCarrey JR. 2020. Unique Epigenetic Programming Distinguishes Regenerative Spermatogonial Stem Cells in the Developing Mouse Testis. *iScience* **23**: 101596.

Danecek P, Bonfield JK, Liddle J, Marshall J, Ohan V, Pollard MO, Whitwham A, Keane T, McCarthy SA, Davies RM, et al. 2021. Twelve years of SAMtools and BCFtools. *Gigascience* **10**: giab008.

Dobin A, Davis CA, Schlesinger F, Drenkow J, Zaleski C, Jha S, Batut P, Chaisson M, Gingeras TR. 2013. STAR: ultrafast universal RNA-seq aligner. *Bioinformatics* **29**: 15–21.

Erkek S, Hisano M, Liang C-Y, Gill M, Murr R, Dieker J, Schübeler D, Vlag J van der, Stadler MB, Peters AHFM. 2013. Molecular determinants of nucleosome retention at CpG-rich sequences in mouse spermatozoa. *Nat Struct Mol Biol* **20**: 868–875.

Ernst J, Kellis M. 2017. Chromatin-state discovery and genome annotation with ChromHMM. *Nat Protoc* **12**: 2478–2492.

Fanourgakis G, Gaspa-Toneu L, Komarov PA, Papasaikas P, Ozonov EA, Smallwood SA, Peters AHFM. 2025. DNA methylation modulates nucleosome retention in sperm and H3K4 methylation deposition in early mouse embryos. *Nat Commun* **16**: 465.

Hammoud SS, Low DHP, Yi C, Carrell DT, Guccione E, Cairns BR. 2014. Chromatin and Transcription Transitions of Mammalian Adult Germline Stem Cells and Spermatogenesis. *Cell Stem Cell* **15**: 239–253.

Heinz S, Benner C, Spann N, Bertolino E, Lin YC, Laslo P, Cheng JX, Murre C, Singh H, Glass CK. 2010. Simple Combinations of Lineage-Determining Transcription Factors Prime cis-Regulatory Elements Required for Macrophage and B Cell Identities. *Mol Cell* **38**: 576–589.

Jung YH, Sauria MEG, Lyu X, Cheema MS, Ausio J, Taylor J, Corces VG. 2017. Chromatin States in Mouse Sperm Correlate with Embryonic and Adult Regulatory Landscapes. *Cell Rep* **18**: 1366–1382.

Kang Z, Xu C, Lu S, Gong J, Yan R, Luo G, Wang Y, He Q, Wu Y, Yan Y, et al. 2025. NKAPL facilitates transcription pause-release and bridges elongation to initiation during meiosis exit. *Nat Commun* **16**: 791.

Kitamura Y, Takahashi K, Maezawa S, Munakata Y, Sakashita A, Kaplan N, Namekawa SH. 2023. CTCF-mediated 3D chromatin predetermines the gene expression program in the male germline. *bioRxiv* 2023.11.30.569508.

Langmead B, Salzberg SL. 2012. Fast gapped-read alignment with Bowtie 2. *Nat Methods* **9**: 357–359.

Lee SM, Loo CE, Prasasya RD, Bartolomei MS, Kohli RM, Zhou W. 2024. Low-input and single-cell methods for Infinium DNA methylation BeadChips. *Nucleic Acids Res* **52**: e38–e38.

Liao Y, Smyth GK, Shi W. 2014. featureCounts: an efficient general purpose program for assigning sequence reads to genomic features. *Bioinformatics* **30**: 923–930.

Liu Y, Zhang Y, Yin J, Gao Y, Li Y, Bai D, He W, Li X, Zhang P, Li R, et al. 2019. Distinct H3K9me3 and DNA methylation modifications during mouse spermatogenesis. *J Biol Chem* **294**: 18714–18725.

Maezawa S, Hasegawa K, Yukawa M, Kubo N, Sakashita A, Alavattam KG, Sin H-S, Kartashov AV, Sasaki H, Barski A, et al. 2018. Polycomb protein SCML2 facilitates H3K27me3 to establish bivalent domains in the male germline. *Proc Natl Acad Sci* **115**: 4957–4962.

Maezawa S, Sakashita A, Yukawa M, Chen X, Takahashi K, Alavattam KG, Nakata I, Weirauch MT, Barski A, Namekawa SH. 2020. Super-enhancer switching drives a burst in gene expression at the mitosis-to-meiosis transition. *Nat Struct Mol Biol* **27**: 978–988.

Margolin G, Khil PP, Kim J, Bellani MA, Camerini-Otero RD. 2014. Integrated transcriptome analysis of mouse spermatogenesis. *BMC Genom* **15**: 39.

Pepin A-S, Jazwiec PA, Dumeaux V, Sloboda DM, Kimmins S. 2024. Determining the effects of paternal obesity on sperm chromatin at histone H3 lysine 4 tri-methylation in relation to the placental transcriptome and cellular composition. *eLife* **13**: e83288.

Ramírez F, Ryan DP, Grüning B, Bhardwaj V, Kilpert F, Richter AS, Heyne S, Dündar F, Manke T. 2016. deepTools2: a next generation web server for deep-sequencing data analysis. *Nucleic Acids Res* **44**: W160–W165.

Ritchie ME, Phipson B, Wu D, Hu Y, Law CW, Shi W, Smyth GK. 2015. limma powers differential expression analyses for RNA-sequencing and microarray studies. *Nucleic Acids Res* **43**: e47–e47.

Siklenka K, Erkek S, Godmann M, Lambrot R, McGraw S, Lafleur C, Cohen T, Xia J, Suderman M, Hallett M, et al. 2015. Disruption of histone methylation in developing sperm impairs offspring health transgenerationally. *Science* **350**: aab2006.

Smith T, Heger A, Sudbery I. 2017. UMI-tools: modeling sequencing errors in Unique Molecular Identifiers to improve quantification accuracy. *Genome Res* **27**: 491–499.

Vara C, Paytuví-Gallart A, Cuartero Y, Dily FL, Garcia F, Salvà-Castro J, Gómez-H L, Julià E, Moutinho C, Cigliano RA, et al. 2019. Three-Dimensional Genomic Structure and Cohesin

Occupancy Correlate with Transcriptional Activity during Spermatogenesis. *Cell Rep* **28**: 352-367.e9.

Wang C, Liu X, Gao Y, Yang L, Li C, Liu W, Chen C, Kou X, Zhao Y, Chen J, et al. 2018. Reprogramming of H3K9me3-dependent heterochromatin during mammalian embryo development. *Nat Cell Biol* **20**: 620–631.

Wang L, Zhang J, Duan J, Gao X, Zhu W, Lu X, Yang L, Zhang J, Li G, Ci W, et al. 2014. Programming and inheritance of parental DNA methylomes in mammals. *Cell* **157**: 979–991. https://linkinghub.elsevier.com/retrieve/pii/S0092867414005340.

Yan R, Cheng X, Gu C, Xu Y, Long X, Zhai J, Sun F, Qian J, Du Y, Wang H, et al. 2022. Dynamics of DNA hydroxymethylation and methylation during mouse embryonic and germline development. *Nat Genet* 1–14.

Yin H, Kang Z, Zhang Y, Gong Y, Liu M, Xue Y, He W, Wang Y, Zhang S, Xu Q, et al. 2021. HDAC3 controls male fertility through enzyme-independent transcriptional regulation at the meiotic exit of spermatogenesis. *Nucleic Acids Res* **49**: 5106–5123.

Zhang Y, Liu T, Meyer CA, Eeckhoute J, Johnson DS, Bernstein BE, Nusbaum C, Myers RM, Brown M, Li W, et al. 2008. Model-based analysis of ChIP-Seq (MACS). *Genome Biol* **9**: R137.

Zhou W, Triche TJ, Laird PW, Shen H. 2018. SeSAMe: reducing artifactual detection of DNA methylation by Infinium BeadChips in genomic deletions. *Nucleic Acids Res* **46**: gky691-.

Zuo X, Rong B, Li L, Lv R, Lan F, Tong M-H. 2018. The histone methyltransferase SETD2 is required for expression of acrosin-binding protein 1 and protamines and essential for spermiogenesis in mice. *J Biol Chem* **293**: 9188–9197.

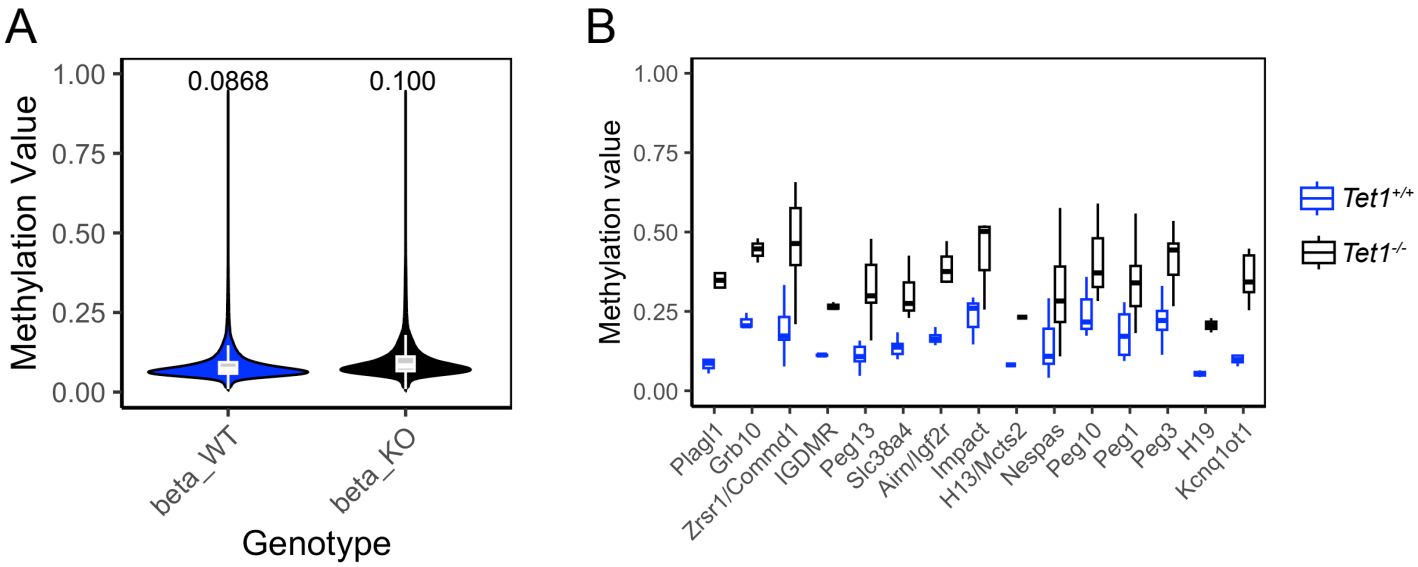

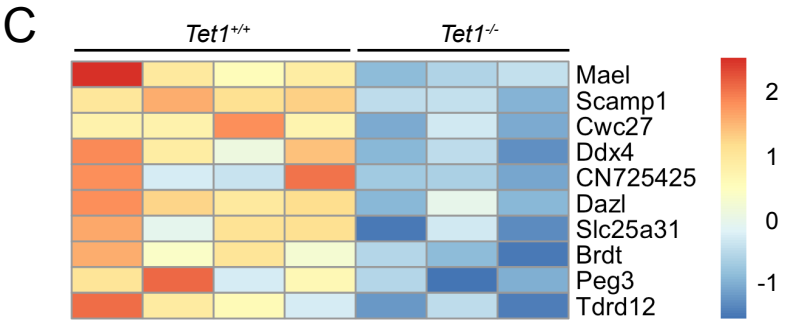

GSE224459; Prasasya et al., 2024

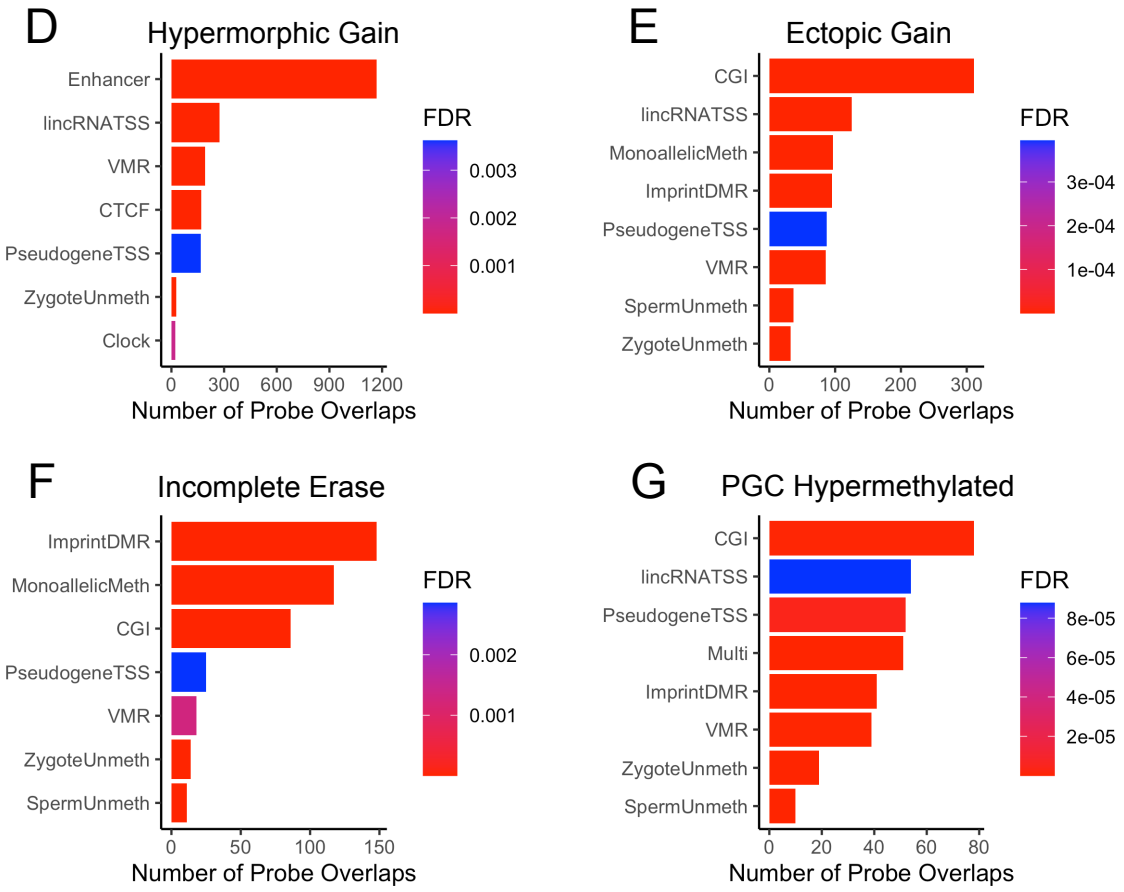

Supplemental Figure 1. Additional analysis of methylation arrays for Tet1-/- vs Tet1+/+ PGCs.

A) Violin plots of average methylation values at each CpG probe with overall mean methylation indicated (n=8 per group). Differentially methylated probes were identified using limma (FDR ≤ 0.05, >10% difference).

B) ICRs are the most enriched design-group category among hypermethylated DMRs in *Tet1*$^{-/-}$ PGCs (15 of 21 array-represented ICRs are significantly hypermethylated). Boxplots show average methylation of probes associated with hypermethylated ICRs.

C–F) Top enriched Infinium Mouse Methylation BeadChip design groups for different categories of *Tet1*$^{-/-}$ sperm and PGC DMRs.

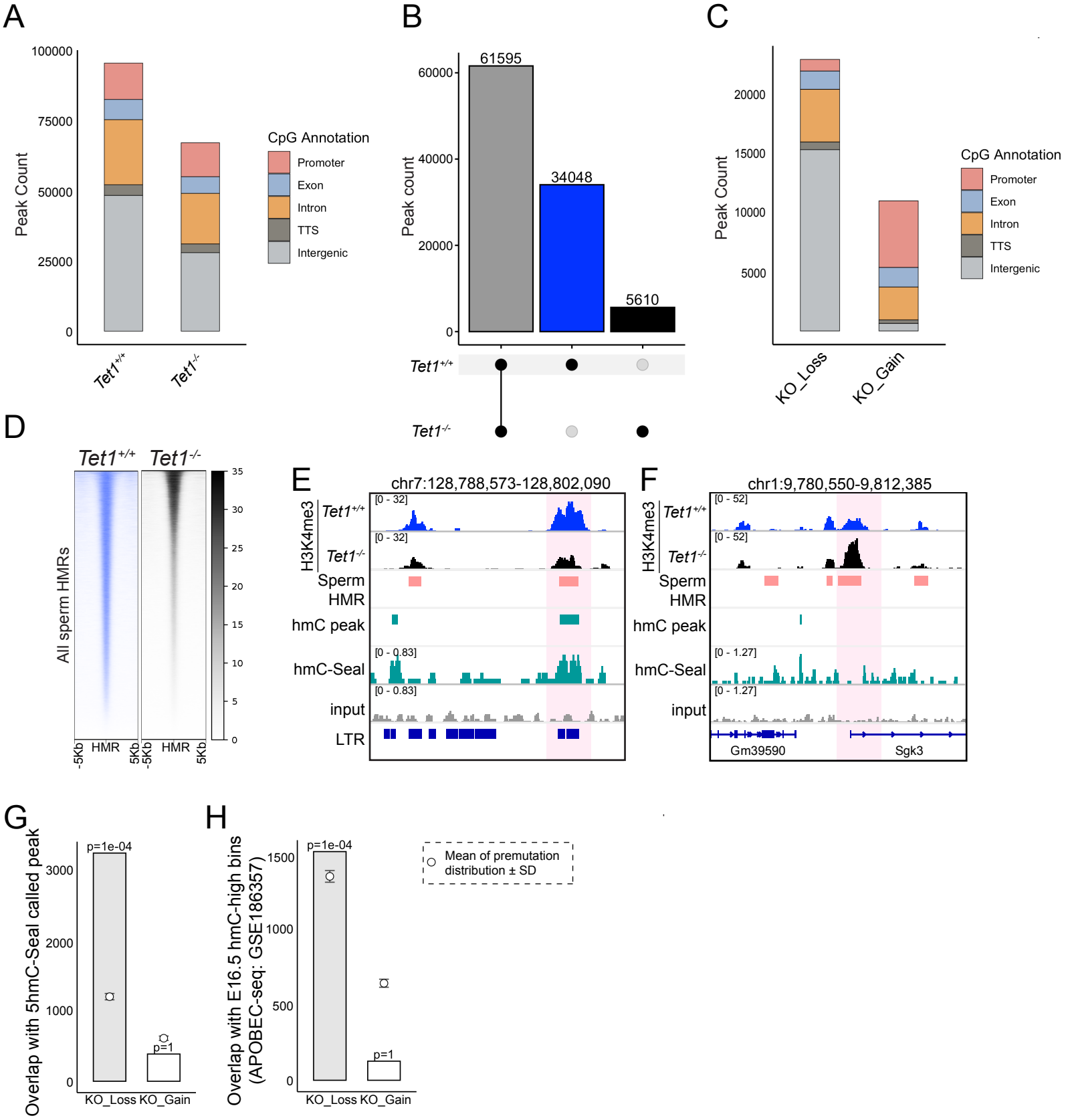
A
Peak Count
100000
75000
50000
25000
0
Tet1+/+
Tet1-/-
CpG Annotation
Promoter
Exon
Intron
TTS
Intergenic
B
Peak count
60000
40000
20000
0
61595
34048
5610
Tet1+/+
Tet1-/-
C
Peak Count
20000
15000
10000
5000
KO_Loss
KO_Gain
CpG Annotation
Promoter
Exon
Intron
TTS
Intergenic
D
Tet1+/+
Tet1-/-
All sperm HMRs
-5Kb
HMR
5Kb
35
30
25
20
15
10
5
0
E
chr7:128,788,573-128,802,090
H3K4me3
Tet1+/+
Tet1-/-
[0 - 32]
Sperm HMR
hmC peak
hmC-Seal
[0 - 0.83]
input
LTR
F
chr1:9,780,550-9,812,385
[0 - 52]
[0 - 1.27]
Gm39590
Sgk3
G
Overlap with 5hmC-Seal called peak
p=1e-04
p=1
KO_Loss
KO_Gain
H
Overlap with E16.5 hmC-high bins (APOBEC-seq: GSE186357)
1500
1000
500
0
Mean of premutation distribution ± SD

Supplemental Figure 2. Additional analysis of differentially enriched H3K4me3 signals in *Tet1*$^{-/-}$ vs *Tet1*$^{+/+}$ prospermatogonia.

A) Genomic compartmentalization of H3K4me3 consensus peaks (present in ≥2 of 3 replicates) in *Tet1*$^{+/+}$ and *Tet1*$^{-/-}$ prospermatogonia.

B)) Distribution of H3K4me3 consensus peaks unique to or shared between *Tet1*$^{+/+}$ (n=3) and *Tet1*$^{-/-}$ (n=3) E17.5 prospermatogonia detected by CUT&RUN.

C) Heatmaps of H3K4me3 signals in E17.5 *Tet1*$^{-/-}$ and *Tet1*$^{+/+}$ prospermatogonia overlapping sperm hypomethylated regions (HMRs) defined by sperm WGBS (GSE56697; Wang et al. 2014). Plots represent averages of 3 biological replicates.

D) Genomic distribution of differentially enriched H3K4me3 peaks between *Tet1*$^{-/-}$ and *Tet1*$^{+/+}$ prospermatogonia (DiffBind, FDR ≤ 0.05, ≥1.5-fold change).

E-F) Genome browser tracks for representative regions showing H3K4me3 loss (E, intergenic) or gain (F, promoter) in *Tet1*$^{-/-}$ prospermatogonia.

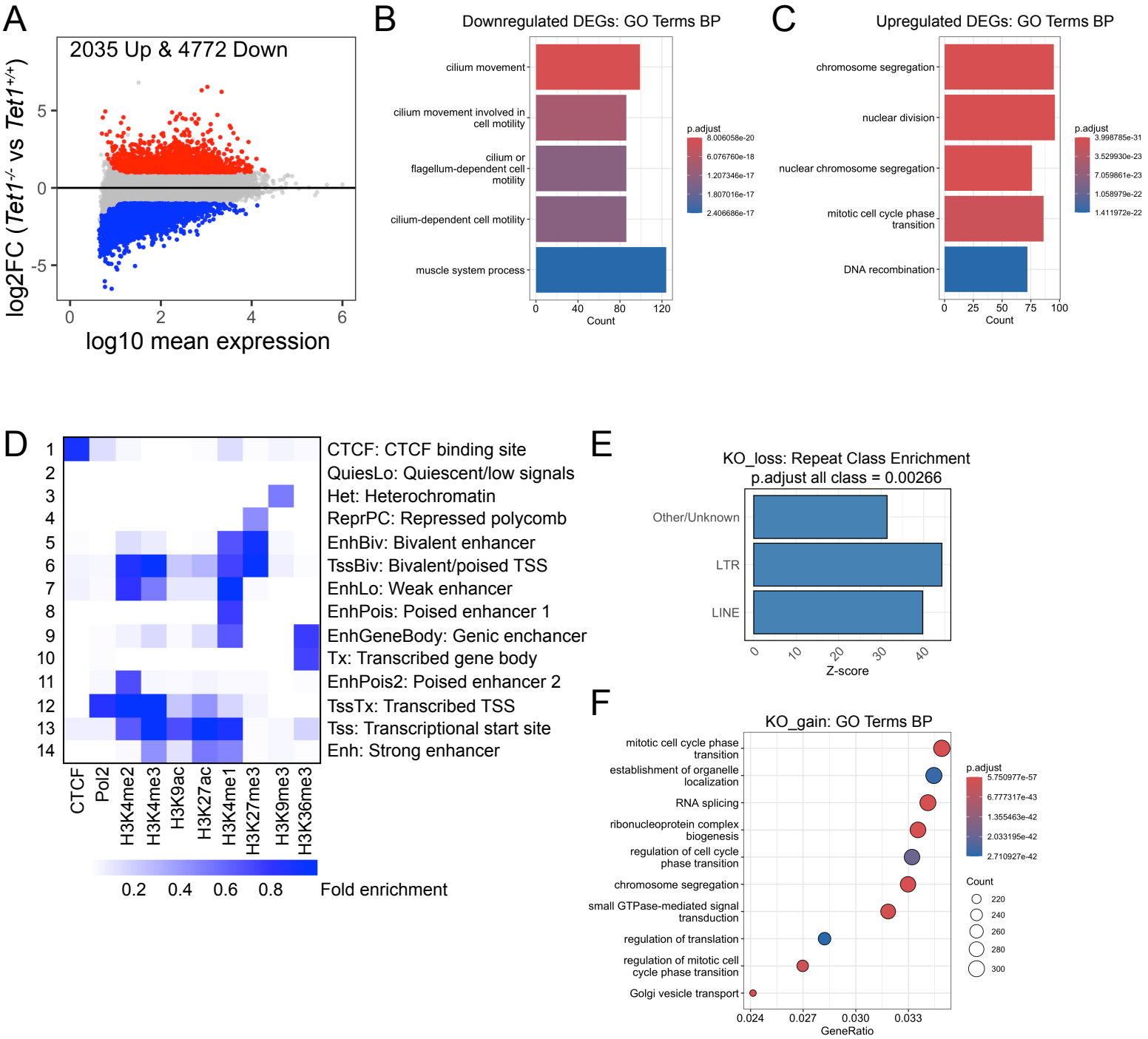
A
2035 Up & 4772 Down
log2FC (Tet1-/- vs Tet1+/+)
log10 mean expression
B
Downregulated DEGs: GO Terms BP
cilium movement
cilium movement involved in cell motility
cilium or flagellum-dependent cell motility
cilium-dependent cell motility
muscle system process
Count
p.adjust
C
Upregulated DEGs: GO Terms BP
chromosome segregation
nuclear division
nuclear chromosome segregation
mitotic cell cycle phase transition
DNA recombination
Count
p.adjust
D
CTCF: CTCF binding site
QuiesLo: Quiescent/low signals
Het: Heterochromatin
ReprPC: Repressed polycomb
EnhBiv: Bivalent enhancer
TssBiv: Bivalent/poised TSS
EnhLo: Weak enhancer
EnhPois: Poised enhancer 1
EnhGeneBody: Genic enchancer
Tx: Transcribed gene body
EnhPois2: Poised enhancer 2
TssTx: Transcribed TSS
Tss: Transcriptional start site
Enh: Strong enhancer
CTCF
Pol2
H3K4me2
H3K4me3
H3K9ac
H3K27ac
H3K4me1
H3K27me3
H3K9me3
H3K36me3
Fold enrichment
E
KO_loss: Repeat Class Enrichment
p.adjust all class = 0.00266
Other/Unknown
LTR
LINE
Z-score
F
KO_gain: GO Terms BP
mitotic cell cycle phase transition
establishment of organelle localization
RNA splicing
ribonucleoprotein complex biogenesis
regulation of cell cycle phase transition
chromosome segregation
small GTPase-mediated signal transduction
regulation of translation
regulation of mitotic cell cycle phase transition
Golgi vesicle transport
GeneRatio
p.adjust
Count

Supplemental Figure 3. Investigation into the potential role of H3K4me3 changes in *Tet1*$^{-/-}$ prospermatogonia

A) MA-plot for differential expression analysis of total RNA-seq in *Tet1*$^{-/-}$ prospermatogonia vs WT (n=3, FDR ≤ 0.05, ≥2-fold change).

B) Top five enriched GO biological process terms for downregulated DEGs in *Tet1*$^{-/-}$ prospermatogonia.

C) Top five enriched GO biological process terms for upregulated DEGs in *Tet1*$^{-/-}$ prospermatogonia.

D) Chromatin states assigned by ChromHMM using public datasets for CTCF, Pol II, and histone modifications across spermatogonial stem cells (SSC), spermatogonia (SPG), pachytene spermatocytes (PS), round spermatids (RS), and sperm (datasets used are in supplemental table). Chromatin state assignment is based on Encode consortium convention (Ernst and Kellis 2017).

E) Classes of repetitive elements enriched in regions with H3K4me3 loss.

F) Top ten enriched GO biological process terms for regions with H3K4me3 gain.

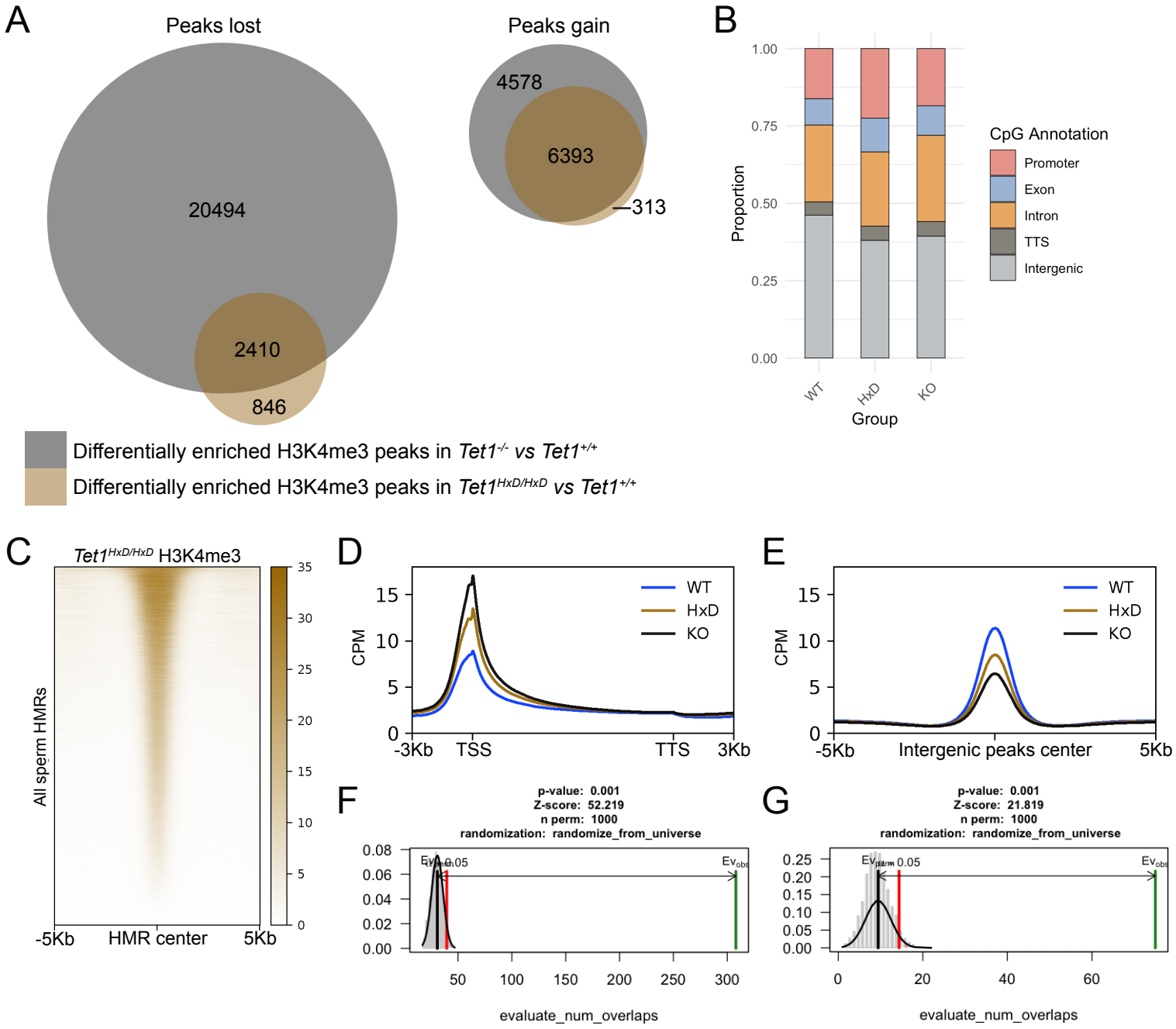
A
Peaks lost
20494
2410
846
Peaks gain
4578
6393
313
B
Proportion
1.00
0.75
0.50
0.25
0.00
WT
HxD
KO
Group
CpG Annotation
Promoter
Exon
Intron
TTS
Intergenic
Differentially enriched H3K4me3 peaks in Tet1-/- vs Tet1+/+
Differentially enriched H3K4me3 peaks in Tet1HxD/HxD vs Tet1+/+
C
Tet1HxD/HxD H3K4me3
All sperm HMRs
-5Kb
HMR center
5Kb
D
CPM
WT
HxD
KO
-3Kb
TSS
TTS
3Kb
E
CPM
WT
HxD
KO
-5Kb
Intergenic peaks center
5Kb
F
p-value: 0.001
Z-score: 52.219
n perm: 1000
randomization: randomize_from_universe
evaluate_num_overlaps
G
p-value: 0.001
Z-score: 21.819
n perm: 1000
randomization: randomize_from_universe
evaluate_num_overlaps

Supplemental Figure 4. Extended CUT&RUN analysis for H3K4me3 in *Tet1*$^{HxD/HxD}$ prospermatogonia.

A) Venn diagrams of differentially enriched peaks in *Tet1*$^{-/-}$ vs *Tet1*$^{+/+}$ and *Tet1*$^{HxD/HxD}$ vs *Tet1*$^{+/+}$ prospermatogonia (DiffBind, FDR ≤ 0.05, ≥1.5-fold change).

B) Genomic compartmentalization of consensus peaks (≥2 of 3 replicates) in *Tet1*$^{+/+}$, *Tet1*$^{HxD/HxD}$, and *Tet1*$^{-/-}$ prospermatogonia.

C) Heatmaps of H3K4me3 signals in E17.5 *Tet1*$^{HxD/HxD}$ prospermatogonia overlapping sperm HMRs defined by WGBS (GSE56697; Wang et al. 2014). Plots represent averages of 3 replicates.

D–E) Metaplots of H3K4me3 signals over genic regions (D) or intergenic consensus peaks (E) for *Tet1*$^{+/+}$, *Tet1*$^{HxD/HxD}$, and *Tet1*$^{-/-}$ prospermatogonia.

F-G) The significance of enrichment of TET1^{HxD}-rescued (F) or TET1^{HxD}-not rescued (G) DMRs within regions where H3K4me3 was restored to WT levels in *Tet1*$^{HxD/HxD}$ prospermatogonia following observed depletion in *Tet1*$^{-/-}$ prospermatogonia. In the graph, the grey-shaded region under the curve represents the distribution of the number of overlaps between 1000 randomized DMRs (within the array coverage) and the fixed set of H3K4me3-restored regions, values above the red line correspond to the area with a significance of $p < 0.05$. The solid green line represents the observed number of overlaps between rescued or not-rescued DMRs and H3K4me3-restored regions. Z-scores represent the strength or standardized magnitude of enrichment of overlap.